Nonlinear Dyn (2015) 79:2675–2698
DOI 10.1007/s11071-014-1840-0

ORIGINAL PAPER

Asymptotic analysis of a noncontact AFM microcantilever sensor with external feedback control

Valeria Settimi · Oded Gottlieb · Giuseppe Rega

Received: 21 May 2014 / Accepted: 3 December 2014 / Published online: 31 December 2014

Abstract An external feedback control is inserted in a nonlinear continuum formulation of a noncontact AFM model. The aim of the feedback is to keep the system response to an operationally suitable one, thus allowing reliable measurement of the sample surface by avoiding possible unstable microcantilever sensor motions. The study of the weakly nonlinear system dynamics about the desired fixed point close to primary resonance is carried out via multiple-scale asymptotics, whose outcomes are validated via numerical simulations of the original system equations of motion. The latter include controllable periodic dynamics and additional periodic and distinct quasiperiodic solutions that appear beyond the asymptotic stability thresholds. The results highlight the effectiveness of the applied feedback control technique and also enable the derivation of a comprehensive system bifurcation structure highlighting the stability thresholds for robust controllable AFM dynamics.

V. Settimi (✉) · G. Rega
Department of Structural and Geotechnical Engineering,
Sapienza University of Rome, Rome, Italy
e-mail: valeria.settimi@uniroma1.it

G. Rega
e-mail: giuseppe.rega@uniroma1.it

O. Gottlieb
Department of Mechanical Engineering,
Technion - Israel Institute of Technology, Haifa, Israel
e-mail: oded@technion.ac.il

Keywords Noncontact AFM · External feedback control · Multiple-scale asymptotics · Stability · Numerical simulation · Bifurcation structure

1 Introduction

A wide variety of phenomena which characterize the atomic force microscope (AFM) microcantilever nonlinear dynamical behavior has been clearly revealed in the last years, and well-known dynamical events, such as bifurcations, in-well instability regions, and eventually chaotic motions, have been experimentally and theoretically documented [1–5]. In particular, the authors have already analyzed the rich nonlinear dynamical behavior of a single-mode model of noncontact AFM proposed by [6] in terms of identification of the bifurcation scenarios and the stability regions as a function of the main system dynamical parameters, and the obtained results have stressed the strong variability of the response when the system operating parameters are slightly modified [7]. As a consequence, strong alterations of the dynamical response can occur, leading to possible unstable, aperiodic, and even chaotic oscillations, which represent an undesirable behavior and cause a restriction to the operating range of many electronic and mechanical systems. Indeed, the calibration of parameters can be influenced by various distortions, due to instrumental noise, thermal fluctuations, artifacts created by the AFM tip, contamination of the mineral or tip surface, and tip-induced surface defor-

mations. These various and complex effects are investigated almost exclusively with experimental analyses [8–11] due to the great difficulty in formulating standard models for phenomena that are closely related to the specific material characteristics and operation of these instruments.

Moreover, for AFMs operating in the noncontact mode, the topography is strongly related to the tip-sample distance, as the tip has to maintain a target distance from the sample so as to ensure that the microcantilever elastic restoring force is stronger than the atomic attraction between tip and sample. Otherwise, instability of the equilibrium configuration occurs, with the so-called jump-to-contact, or escape (in dynamical systems terms) phenomenon. During the scan operation, however, the sample roughness can modify the distance between the microcantilever tip and the sample to be scanned, and thus, the nonlinear atomic force interaction which is used to obtain the topography can lead to unstable dangerous motions as sketched in the following Sect. 1.1. To prevent these undesirable motions, several control techniques have been proposed in the field of AFMs during the last two decades, primarily based on the feedback control methods [12–20]. Among them, Yagasaki [21] has recently applied the external feedback control technique proposed by Pyragas [22] to a simple tapping AFM model that works by keeping the microcantilever vibration to a selected reference one and allowing to simultaneously and reliably measure the sample surface.

The aim of this work is to implement a control procedure within a nonlinear model of noncontact AFM well established in the literature, in order to assess its effects on the system dynamics and to critically evaluate its actual effectiveness in the selected operation conditions of air and weak vacuum.

For this purpose, the feedback control method proposed by Yagasaki [21,23] is introduced at the outset of the continuum-based noncontact AFM nonlinear model formulation by Hornstein and Gottlieb [6]; in particular, the periodic motion used as a reference in the control procedure is chosen to be the response of the corresponding uncontrolled system, for which the analysis presented in Rega and Settimi [7] has already allowed detection of the main stability regions for the most relevant parameters combinations. Following the existence and stability analysis of the controlled system equilibria, the effectiveness of the procedure in the weakly nonlinear regime is checked via the asymptotic multiple-scale method, which yields a reduced set of differential equations governing the slow-time amplitudes of motion. The slow dynamics are compared with the results obtained by numerical integration of the original system equations. Throughout the study, the analysis of the controlled system is compared with the underlying uncontrolled one.

The paper is organized as follows. Continuous and reduced-order modeling of the dynamics of controlled system is addressed in Sect. 2. A high-order multiple-scale analysis of weakly nonlinear dynamics is accomplished in Sect. 3. Section 4 is devoted to verification of the control effectiveness in maintaining the desired system response, and to numerically validating the possible outcomes of the asymptotic approximation culminating with the controlled system bifurcation structure. The paper ends with some conclusions.

1.1 Influence of the tip-sample distance on the dynamics of a single-mode model

Referring to the single-mode model of a nonlinear noncontact AFM microcantilever derived and analyzed asymptotically in Hornstein and Gottlieb [6] and analyzed numerically in Rega and Settimi [7] (see Fig. 2a forward), it is of interest to investigate the changes in the system response as a function of the varying tip-sample gap. To this end, a new nondimensional parameter δ_g, which represents the possible changes in the tip-sample distance, is introduced into the atomic interaction term of the reduced-order equation of motion (22) of Hornstein and Gottlieb [6]:

$$\begin{aligned}\left(1+\alpha_2 x^2\right)\ddot{x}+\left(\alpha_1+\alpha_2\dot{x}^2+\alpha_3 x^2\right)x \\ =-\frac{\Gamma_1}{\left(1-\delta_g+x+V_g\right)^2}-\left(\rho_1+\rho_2 x^2\right)\dot{x} \\ -\left(\ddot{V}_g+\nu_1\dot{V}_g\right)\nu_2 \\ +\left(\mu_1 x+\mu_2 x^3\right)\left(\ddot{U}_g+\eta_1\dot{U}_g+\eta_2 U_g\right)\end{aligned} \tag{1}$$

where $\delta_g=\bar{\delta_g}/\gamma$ is the nondimensional reduction ratio of the tip-sample gap. For the meaning of the various quantities, see Sect. 2.1.

Bifurcation diagrams of Fig. 1a, b are obtained for the parametrically excited ($V_g=0$, $U_g=U\sin(\omega_u t)$) AFM model near the fundamental resonance and for the following set of parameter values: $\alpha_1=1$, $\alpha_3=0.1$, $\rho_1=0.001$, $\Gamma_1=0.1$,$\mu_1=1.5708$, $\omega_u=0.76$.

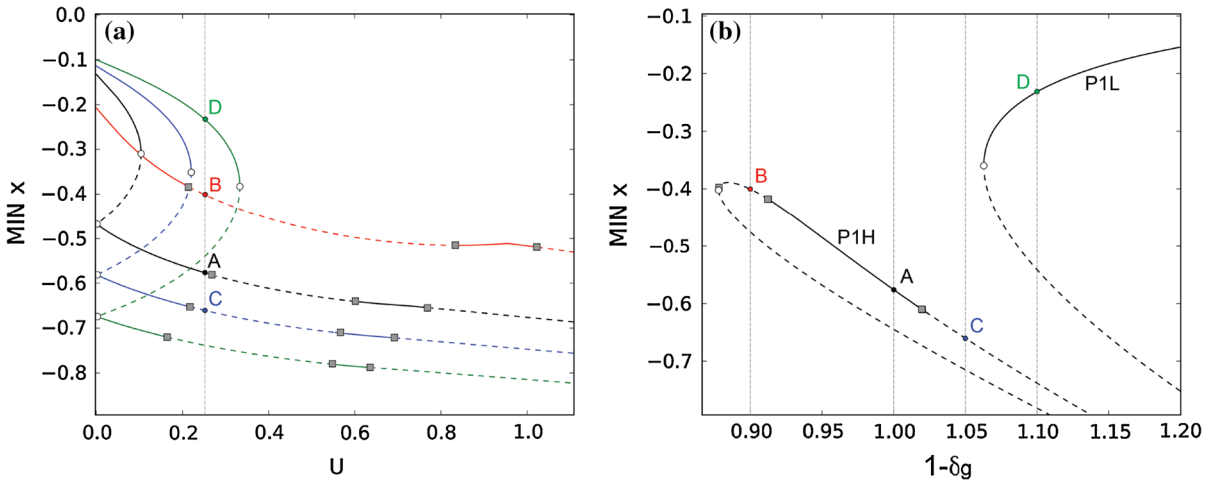

Fig. 1 Bifurcation diagrams as a function of the forcing amplitude U for $\delta_g = 0$ (*black line*), $\delta_g = 0.1$ (*red line*), $\delta_g = -0.05$ (*blue line*), and $\delta_g = -0.1$ (*green line*) (**a**); bifurcation diagram as a function of the tip-sample gap at $U = 0.25$ (**b**), for $\omega_u = 0.76$. *Gray square* period doubling bifurcation; *White circle* saddle-node bifurcation; P1L low-amplitude 1-period solution; P1H high-amplitude 1-period solution. (Color figure online)

The results clearly highlight that the tip-sample gap strongly modifies the dynamical behavior of the AFM microcantilever, changing the regions of existence and/or stability of the main periodic solutions (i.e., low-amplitude P1L solution and high-amplitude P1H solution defined in Fig. 1). This means that during the horizontal scan operations that incorporate changes in tip-sample distance, the dynamical response of the microcantilever can suddenly pass from low-amplitude oscillations (point D in Fig. 1) to high-amplitude motions (point A in Fig. 1) and eventually bring to unstable periodic solutions (points B and C in Fig. 1), the last ones representing unwanted responses that entail erroneous results on the sample topography.

2 Modeling

2.1 Equations of motion and reduced-order model

The physical model at the base of the work is a fixed-free AFM microcantilever, which is assumed to be planar, inextensible, and horizontal, with length L and a sharp tip of height h_T close to its free end, and with a distance g between its fixed side and the sample (Fig. 2a). The beam material is considered linearly elastic, homogeneous, and isotropic, with Young's modulus E. The general formulation of Hornstein and Gottlieb [6], based on the classical inextensional beam model of Crespo da Silva and Glynn [24], is referred to, and following the method proposed by Yagasaki [21], a stable periodic response of the mentioned AFM model is chosen as the reference one. The corresponding positions of the oscillating microcantilever base and of the sample surface represent consequently the reference configuration (see Fig. 2a). When the microcantilever response changes due to variations in the sample surface position, the external feedback control acts by keeping it to the reference one thanks to the control of the microcantilever base position. A new parameter $\bar{\xi}_s$ is thus introduced, which is the displacement of the sample surface from the selected reference position, while the new variable $\bar{\xi}(t)$ represents the distance of the fixed side of the microcantilever from the horizontal reference axis (Fig. 2b).

Differently from the procedure followed by Yagasaki, who inserted the control into the reduced single-mode model of tapping AFM, in this work, the control is introduced at the very beginning of the model formulation; accordingly, a new d.o.f. is added to the general relations of the uncontrolled system [6]:

$$
\begin{aligned}
&m\bar{u}_{tt} - [EI\bar{v}_{rrr}\bar{v}_r - J_z\bar{v}_{ttr}\bar{v}_r + \Lambda(1+\bar{u}_r)]_r = \bar{Q}_u \\
&m\bar{v}_{tt} - [EI(\bar{v}_{rrr} + \bar{v}_r\bar{v}_{rr}^2) \\
&\quad + J_z(\bar{v}_{ttr} + \bar{v}_{tr}^2\bar{v}_r) + \Lambda\bar{v}_r]_r = \bar{Q}_v \\
&\bar{\xi}_t = \bar{k}(\bar{v}_{ref} - \bar{v})
\end{aligned}
\tag{2}
$$

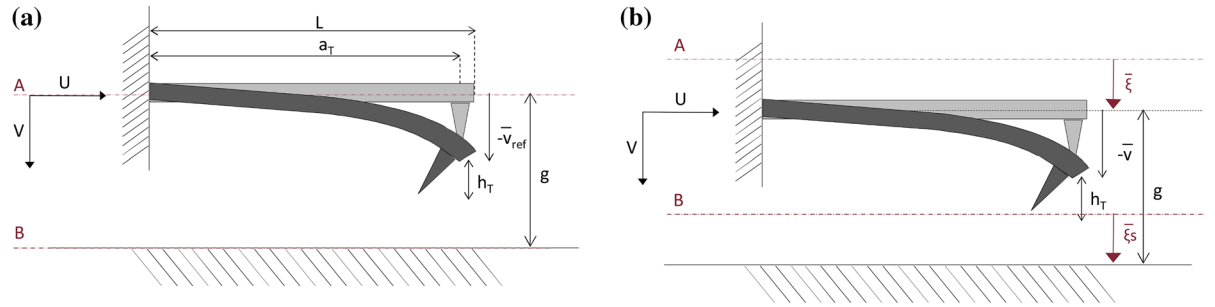

Fig. 2 Microcantilever at reference position (**a**) and in a generic configuration (**b**); lines A and B represent the reference positions of the microcantilever and the sample surface, respectively. (Color figure online)

where coefficients EI, J_z, and m are the beam flexural stiffness, principal mass moment of inertia about z, and mass per unit reference length, respectively; Λ is a Lagrange multiplier accounting for the inextensibility condition; and subscript letters denote partial differentiation with respect to the arc-length r and time t. $\bar{u}(r,t)$ and $\bar{v}(r,t)$ are now the horizontal and vertical displacements of the controlled system; $\bar{v}_{ref}(r,t)$ represents the reference vertical displacement, obtained from the uncontrolled system ($\bar{\xi}=0$); and $\bar{k}$ is a feedback constant. The generalized forces in horizontal and vertical directions $\bar{Q}_u$ and $\bar{Q}_v$ are

$$\begin{aligned}\bar{Q}_u &= -\bar{g}_1\dot{\bar{u}}_t - \bar{g}_2\dot{\bar{u}}_{trr} - \bar{g}_3\dot{\bar{u}}\\ \bar{Q}_v &= \delta(r-a_T)F_v^A - d\dot{\bar{v}}_t\end{aligned} \tag{3}$$

the latter also accounting for the localized (at $r=a_T$, see Fig. 2a) transverse atomic force interaction F_v^A, derived from the phenomenological Lennard-Jones (LJ) potential [25–27] for a sphere-plane system. The LJ potential is extensively used in the AFM literature to derive the atomic interaction force, as it takes into account both the attractive and the repulsive contributions (see, e.g., [14,15,18]). It is noteworthy that a variety of methods have been used to estimate the Hamaker constant governing the force derived from the LJ potential [28,29], and recently, a novel strategy was demonstrated for appropriate selection of van der Waals force interactions, thus enabling experimental-based model verification [30]. As LJ potential is dependent on the tip-sample distance g, its expression is modified by the external feedback control as follows

$$F_v^A = \frac{A_H R_T}{6\sigma_a^2}\left[-\left(\frac{\sigma_a}{g+\bar{v}-h_T-\bar{\xi}_s}\right)^2 + \frac{1}{30}\left(\frac{\sigma_a}{g+\bar{v}-h_T-\bar{\xi}_s}\right)^8\right] \tag{4}$$

The term out of parenthesis on the right side is the magnitude of the potential in terms of Hamaker constant A_H and tip radius R_T, while the term in parenthesis describes the shape of the potential in terms of the actual tip-sample distance g and a typical atomic distance σ_a. $\bar{g}_1$, $\bar{g}_2$, and $\bar{g}_3$ are coefficients related to linear viscous damping, material viscoelastic damping, and a proportional displacement gain, respectively, while d is a viscous damping coefficient and δ is the Dirac delta. The new variable $\bar{\xi}(t)$ modifies the boundary conditions as follows:

$$\begin{aligned}&\bar{v}(0,t) = \bar{V}(t)+\bar{\xi}(t) = \bar{W}(t), \quad \bar{v}_r(0,t)=0,\\ &\bar{u}(0,t) = \bar{U}(t), \quad \bar{v}_{rr}(L,t)=0, \quad \bar{v}_{rrr}(L,t)=0,\\ &\bar{u}_r(L,t)=0.\end{aligned} \tag{5}$$

with $\bar{V}(t)$ and $\bar{U}(t)$ the vertical transverse and horizontal scan displacement, respectively. The holonomic inextensibility constraint ($(1+\bar{u}_r)^2+\bar{v}_r^2=1$) integration and incorporation in the horizontal boundary conditions yields

$$\bar{u}(r) = \bar{U}(t) - \int_0^r \bar{v}_r^2 \mathrm{d}r \tag{6}$$

Its substitution in the first equation of (2) and the subsequent integration of the partial integro-differential equation allow one to isolate the Lagrangian multiplier

$$\Lambda = \left(1-\frac{1}{2}\bar{v}_r^2\right)^{-1}\left[J_z\dot{\bar{v}}_{trr}\bar{v}_r - EI\bar{v}_{rrr}\bar{v}_r + m\int_L^r \ddot{\bar{U}}_{tt}\mathrm{d}r - \frac{m}{2}\int_L^r \frac{\mathrm{d}^2}{\mathrm{d}t^2}\left(\int_0^r \bar{v}_r^2\mathrm{d}r\right)\mathrm{d}r - \int_L^r \bar{Q}_u\mathrm{d}r\right] \tag{7}$$

Rescaling the boundary problem by its length L ($s=r/L$) and time ($\tau=\omega_s t$) by a standard characteristic frequency $\omega_s=\sqrt{EI/mL^4}$, expanding the multiplier up to the cubic order, substituting into the nondimensional form of the second of (2), and transforming the nondimensional system to a moving reference frame

$$v(s,\tau) = w(s,\tau) + V(\tau) \tag{8}$$

yield

$$\begin{aligned} &w_{\tau\tau} + W_{\tau\tau} + w_{ssss} - \mu w_{\tau\tau ss} - Q_w \\ &= \Bigg[-w_s\,(w_{ss}w_s)_s + \mu w_s\,(w_{\tau s}w_s)_\tau \\ &\quad + w_s\left(\left(1+\frac{1}{2}w_s^2\right)\int_1^s U_{\tau\tau}\mathrm{d}s \right. \\ &\quad - \frac{1}{2}\int_1^s \left(\int_0^s w_s^2\mathrm{d}s\right)_{\tau\tau}\mathrm{d}s \\ &\quad \left. - \left(1+\frac{1}{2}w_s^2\right)\int_1^s Q_u\mathrm{d}s\right)\Bigg]_s \\ &\xi_\tau = k(w_{ref} - w) \end{aligned} \tag{9}$$

where

$$\begin{aligned} Q_u = &-g_1\left[U_\tau(\tau) - \frac{1}{2}\frac{\partial}{\partial\tau}\left(\int_0^s w_s^2\mathrm{d}s\right)\right] \\ &+ \frac{1}{2}g_2\left[\frac{\partial^3}{\partial\tau\partial s^2}\left(\int_0^s w_s^2\mathrm{d}s\right)\right] \\ &- g_3\left[U(\tau) - \frac{1}{2}\int_0^s w_s^2\mathrm{d}s\right] \end{aligned} \tag{10}$$

and the generalized force in vertical direction Q_v is modified by the boundary conditions (5) as follows:

$$\begin{aligned} Q_w = \delta(s-\alpha)\bar{\Gamma}_1\Bigg[&-\frac{1}{(\gamma + w + W - \xi_s)^2} \\ &+\frac{\bar{\Gamma}_2}{(\gamma + w + W - \xi_s)^8}\Bigg] - v(w_\tau + B_\tau) \end{aligned} \tag{11}$$

with $\xi = \bar{\xi}/L$, $\xi_s = \bar{\xi}_s/L$, $k = \bar{k}/L$, $W = \bar{W}/L$, $w_{ref} = \bar{v}_{ref}/L$, and

$$\begin{aligned} &v = \bar{v}/L, \quad v_s = \bar{v}_r, \quad v_{ss} = \bar{v}_{rr}/L, \quad v_{sss} = \bar{v}_{rrr}/L^2, \\ &Q_u = L^3\bar{Q}_u/EI, \quad Q_v = L^3\bar{Q}_v/EI, \quad \mu = J_z/mL^2, \\ &U(\tau) = \bar{U}/L, \quad V(\tau) = \bar{V}/L, \quad g_1 = \bar{g}_1L^4\omega_s/EI, \\ &g_2 = \bar{g}_2L^2\omega_s/EI, \quad g_3 = \bar{g}_3L^4\omega_s/EI, \quad \nu = d\omega_sL, \\ &\bar{\Gamma}_1 = A_HR_T/6EI, \quad \bar{\Gamma}_2 = (\sigma_aL)^6/30, \\ &\alpha = a_T/L, \quad \gamma = (g - h_T)/L. \end{aligned} \tag{12}$$

g_1, g_2, and g_3 are controller's constants, $\bar{\Gamma}_1$ and $\bar{\Gamma}_2$ are nondimensional atomic force constants, α is the nondimensional distance between tip and microbeam fixed end, γ is the nondimensional gap distance, and ν is the nondimensional damping coefficient. A set of homogeneous boundary conditions completes the problem formulation

$$\begin{aligned} &w(0,\tau) = 0, \quad w_s(0,\tau) = 0, \\ &w_{ss}(1,\tau) = 0, \quad w_{sss}(1,\tau) = 0. \end{aligned} \tag{13}$$

As proposed for the uncontrolled case [6], a single-mode reduction is applied to the controlled vertical displacement variable $w(s,\tau)$ and to the reference vertical displacement $w_{ref}(s,\tau)$

$$\begin{aligned} w(s,\tau) &= q_1(\tau)\Phi_1(s) \\ w_{ref}(s,\tau) &= q_{ref1}(\tau)\Phi_1(s) \end{aligned} \tag{14}$$

where the basis function is that of a clamped-spring beam. The Galerkin procedure leads to the following governing equations

$$\begin{aligned} &I_1q_{1\tau\tau} + I_{11}(\nu q_{1\tau} + \omega_1^2q_1) + I_2(W_{\tau\tau} + \nu W_\tau) + I_3q_1^3 \\ &\quad + I_4q_1\left(q_{1\tau}^2 + q_{1\tau\tau}q_1\right) = q_1^2q_{1\tau}\,(g_1I_{41} + g_2I_7) \\ &\quad + \frac{1}{2}q_1^3I_{41}g_3 - \bar{\Gamma}_1\Phi_1(\alpha)\left(\frac{1}{(\gamma + q_1\Phi_1(\alpha) + B - \xi_s)^2}\right) \\ &\quad + \left(q_1I_5 + \frac{1}{2}q_1^3I_6\right)(U_{\tau\tau} + g_1U_\tau + g_3U) \\ &I_2\xi_\tau = I_{11}k\left(q_{ref1} - q_1\right) \end{aligned} \tag{15}$$

where I_{ij} are the same of the uncontrolled case reported in "Appendix 1," and the repulsion interaction $\bar{\Gamma}_1$ has been neglected due to the noncontact regime of operation of the AFM.

New variables $x(\tau) = q_1(\tau)\Phi_1(\alpha)/\gamma$, $z = \xi/\gamma$, and $x_{ref}(\tau) = q_{ref1}(\tau)\Phi_1(\alpha)/\gamma$ are defined, which are rescaled by the timescale $t_N = \omega_1\tau$, to obtain the final form of the controlled system equations

$$\begin{aligned} &\left(1 + \alpha_2x^2\right)\ddot{x} + \left(\alpha_1 + \alpha_2\dot{x}^2 + \alpha_3x^2\right)x \\ &\quad = -\frac{\Gamma_1}{\left(1 + x + V_g + z - z_s\right)^2} - \left(\rho_1 + \rho_2x^2\right)\dot{x} \\ &\quad - \left(\ddot{V}_g + k_g\left(\dot{x}_{ref} - \dot{x}\right) + \nu_1\left(\dot{V}_g + k_g\left(x_{ref} - x\right)\right)\right)\nu_2 \\ &\quad + \left(\mu_1x + \mu_2x^3\right)\left(\ddot{U}_g + \eta_1\dot{U}_g + \eta_2U_g\right) \\ &\dot{z} = k_g\left(x_{ref} - x\right) \end{aligned} \tag{16}$$

where

$$\begin{aligned} &\alpha_1 = \frac{I_{11}}{I_1}, \quad \alpha_2 = \frac{\gamma^2I_4}{\Phi_1(\alpha)I_1}, \\ &\alpha_3 = \frac{\gamma^2}{\Phi_1^2(\alpha)\omega_1^2}\left(\frac{I_3}{I_1} + \frac{g_3I_{41}}{2I_1}\right), \\ &\Gamma_1 = \bar{\Gamma} - 1\frac{\Phi_1^2(\alpha)}{\gamma^3\omega_1^2I_1}, \quad \mu_1 = \frac{I_5\gamma}{I_1}, \quad \mu_2 = \frac{I_6\gamma^3}{2\Phi_1^2(\alpha)I_1}, \end{aligned}$$

$$\rho_1 = \frac{\nu I_{11}}{\omega_1 I_1},\ \rho_2 = \frac{\gamma^2}{\Phi - 1^2(\alpha)}\left(\frac{g_1 I_{41}}{\omega_1 I_1}\frac{g_2 I_7}{\omega_1 I_1}\right),$$
$$\eta_1 = \frac{g_1}{\omega_1},\ \eta_2 = \frac{g_3}{\omega_1},\ \nu_1 = \frac{\nu}{\omega_1},\ \nu_2 = \frac{I_2 \Phi_1(\alpha)}{I_1},$$
$$V_g = \frac{W}{\gamma},\ U_g = \frac{U(\tau)}{\gamma},\ z_s = \frac{\xi_s}{\gamma},\ k_g = \frac{I_{11} k}{\Phi_1(\alpha) I_2 \omega_1}. \tag{17}$$

x and z are the transverse displacement variable and the newly inserted control variable, respectively; α_1 and α_2 represent linear and nonlinear geometric terms; ρ_1 is the linear damping coefficient, and Γ_1 is the attractive atomic interaction coefficient. U_g and V_g are horizontal and vertical excitations, respectively, that are supposed to be harmonic ($U_g = U\sin(\omega_u t)$, $V_g = V\sin(\omega_v t)$); η_1, η_2, and ρ_2 are feedback control parameters related to the time-dependent horizontal scan and the nonlinear correction to the damping term, respectively; the coefficient α_3 of the cubic stiffness term is also affected by the horizontal control gain. Compared with the uncontrolled system equation [6], it is evident that, as expected, the feedback control acts on the system by modifying the terms related to the tip-sample distance, which are the nonlinear atomic interaction term and the vertical vibration V. Finally, k_g is the external feedback control parameter, and x_{ref} represents the periodic reference response of the uncontrolled system and thus can be expressed as the sum of a mean $\bar{x}_{ref}$ and a time-dependent oscillating component $\tilde{x}_{ref}(t)$

$$x_{ref} = \bar{x}_{ref} + \tilde{x}_{ref}(t) \tag{18}$$

2.2 Equilibrium analysis and stability of fixed points

The equilibrium analysis of the controlled system involves the elimination of the explicit time-dependent excitations $U_g = V_g = 0$ together with the oscillating reference position $\tilde{x}_{ref}(t) = 0$ so that $x_{ref} = \bar{x}_{ref}$

$$\begin{aligned}
\dot{x} &= y \\
\dot{y} &= -\frac{1}{1+\alpha_2 x^2}\Big(\left(\alpha_1 + \alpha_2 y^2 + \alpha_3 x^2\right) x \\
&\quad + \frac{\Gamma_1}{(1+x+z-z_s)^2} + \left(\rho_1 + \rho_2 x^2\right) y \\
&\quad + \left(-y + \nu_1\left(\bar{x}_{ref} - x\right)\right) k_g \nu_2\Big) \\
\dot{z} &= k_g\left(\bar{x}_{ref} - x\right)
\end{aligned} \tag{19}$$

To obtain the system fixed points, the velocities are set equal to zero ($\dot{x} = \ddot{x} = \dot{z} = 0$); consequently, $x = \bar{x}_{ref}$, and $z = z_s$ is the arbitrary displacement from the reference position. The controlled system becomes

$$(1+x)^2\left(\alpha_1 + \alpha_3 x^2\right) x + \Gamma_1 = 0 \tag{20}$$

whose solution $x_e\left(\bar{x}_{ref}, z_s\right)$ points out that the system equilibria are not influenced by the feedback control parameter k_g.

For a general choice of the parameters, the five solutions are obtained from a quintic polynomial which is the same as that of the uncontrolled system; among them, only two solutions are acceptable and correspond to the upper stable fixed point and to the unstable one of the uncontrolled system [6].

The stability of the system fixed points involves the study of the Jacobian matrix at the equilibrium $\mathbf{x_e}\left(\bar{x}_{ref}, z_s\right)$:

$$\mathbf{J}_{\mathbf{x_e}} = \begin{bmatrix} 0 & 1 & 0 \\ a_{21} & a_{22} & a_{23} \\ -k_g & 0 & 0 \end{bmatrix} \tag{21}$$

where

$$\begin{aligned}
a_{21} &= \left(1+\alpha_2\bar{x}_{ref}^2\right)^{-2}\Big(\left(1+\alpha_2\bar{x}_{ref}^2\right)\alpha_1 \\
&\quad - \bar{x}_{ref}^2\left(3+\alpha_2\bar{x}_{ref}^2\right)\alpha_3 \\
&\quad + 2\Gamma_1\left(1+\bar{x}_{ref}\right)^{-3}\left(1+\alpha_2\bar{x}_{ref}\left(1+2\bar{x}_{ref}\right)\right) \\
&\quad + \nu_1\nu_2 k_g\left(1+\alpha_2\bar{x}_{ref}^2\right)\Big) \\
a_{22} &= \left(1+\alpha_2\bar{x}_{ref}^2\right)^{-1}\left(\rho_1 + \rho_2\bar{x}_{ref}^2 - \nu_2 k_g\right) \\
a_{23} &= 2\Gamma_1\left(1+\alpha_2\bar{x}_{ref}^2\right)^{-1}\left(1+\bar{x}_{ref}\right)^{-3}
\end{aligned} \tag{22}$$

The coefficients of its characteristic polynomial $p_{\mathbf{J_{x_e}}}(\lambda) = \lambda^3 + C_1\lambda^2 + C_2\lambda + C_3 = 0$ are

$$\begin{aligned}
C_1 &= -\mathrm{tr}\left(p_{J_{x_e}}\right) = -a_{22} \\
C_2 &= \mathrm{Z}\left(p_{J_{x_e}}\right) = -a_{21} \\
C_3 &= -\det\left(p_{J_{x_e}}\right) = -a_{23}k_g \\
\Delta_2 &= C_1 C_2 - C_3
\end{aligned} \tag{23}$$

The equilibrium solutions are asymptotically stable if and only if

$$\begin{cases} C_j > 0, \quad j = 1,2,3 \\ \Delta_2 > 0 \end{cases} \tag{24}$$

Due to the dependence on the feedback parameter k_g, the stability analysis of the two fixed points has been

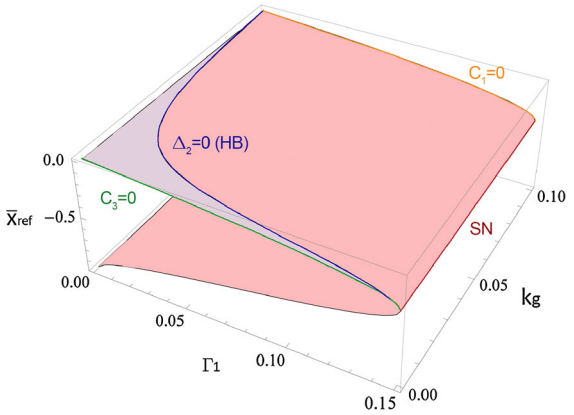

Fig. 3 Stability regions of the controlled fixed points as a function of the feedback control parameter k_g and the atomic interaction parameter Γ_1. *Gray area* = stable region, *red area* = unstable region. (Color figure online)

carried out in function of both Γ_1 and k_g for the following set of parameters values

$$\begin{aligned}&\alpha_1 = 1,\ \alpha_2 = 0,\ \alpha_3 = 0.1,\ \rho_1 = 0.001,\ \rho_2 = 0,\\ &\nu_1 = 0.01,\ \nu_2 = 0.01,\ \mu_1 = 1.5708,\ \mu_2 = 0,\\ &\eta_1 = 0,\ \eta_2 = 0,\ z_s = 0.01\end{aligned} \tag{25}$$

corresponding to those chosen for the uncontrolled system [6]. The reported results are evaluated numerically, with the values of the equilibrium position $\mathbf{x_e}\left(\bar{x}_{ref}, z_s\right)$ obtained as solution of the corresponding uncontrolled system. Figure 3 shows the summarized contributions of the coefficients of the characteristic polynomial (23) governing the stability of the system stable equilibrium solution together with the ones related to the unstable equilibrium branch. The Δ_2 coefficient governs the fixed point stability, reducing it as the value of the feedback control parameter increases, up to the upper boundary of $k_g = 0.1$ for which both Δ_2 and C_1 change their sign making the fixed point unstable. As regards the equilibrium that corresponds to the unstable equilibrium of the uncontrolled system, it remains unstable over the whole domain even after the control introduction.

For the parameters choice (25) and for $\Gamma_1 = 0.1$, which corresponds to the value used for the further numerical analyses, the asymptotic stability of the equilibrium solution occurs for $0 < k_g < 0.00223$. The three eigenvalues which are solution of the characteristic polynomial $p_{\mathbf{J_{x_e}}}$ can be studied to point out the possible bifurcation scenarios of the system fixed points. As they turn out to be $\lambda_{1,2} = \mathrm{Re}_{1,2} \pm i\,\mathrm{Im}_{1,2}$, $\lambda_3 = \mathrm{Re}_3$, it results that a Hopf bifurcation occurs for $\mathrm{Re}_{1,2} = 0$, that is, $\Delta_2 = 0$; as a consequence, the equilibrium stability of the controlled system is now governed by a Hopf bifurcation locus, which occurs for considerably lower values of the atomic interaction parameter with respect to the saddle-node locus which governed the stability of the uncontrolled system.

3 Asymptotic analysis

To validate the applied feedback control technique, and to study the system nonlinear dynamics around the previously obtained fixed point close to primary resonance, the method of multiple scales [31] is applied to the system (16). To this aim, the equations of motions are analyzed around the reference position (x_{ref}, z_s), that is, $y = x - x_{ref} = x - \bar{x}_{ref} - \tilde{x}_{ref}$ and $p = z - z_s$:

$$\begin{aligned}\ddot{y} = &-\frac{1}{\left(1+\alpha_2(y+\bar{x}_{ref}+\tilde{x}_{ref})^2\right)}\\ &\times\left(\alpha_1+\alpha_2\dot{y}^2+\alpha_3(y+\bar{x}_{ref}+\tilde{x}_{ref})^2\right)(y+\bar{x}_{ref}+\tilde{x}_{ref})\\ &+\frac{\Gamma_1}{\left(1+(y+\bar{x}_{ref}+\tilde{x}_{ref})+V_g+p\right)^2}\\ &+\left(\rho_1+\rho_2(y+\bar{x}_{ref}+\tilde{x}_{ref})^2\right)\left(\dot{y}+\dot{\tilde{x}}_{ref}\right)\\ &+\left(\ddot{V}_g-k_g\dot{y}+\nu_1\left(\dot{V}_g-k_g y\right)\right)\nu_2\\ &-\left(\mu_1(y+\bar{x}_{ref}+\tilde{x}_{ref})+\mu_2(y+\bar{x}_{ref}+\tilde{x}_{ref})^3\right)\\ &\times\left(\ddot{U}_g+\eta_1\dot{U}_g+\eta_2 U_g\right)\\ \dot{p} = &-k_g y\end{aligned} \tag{26}$$

with $V_g = V\sin(\omega_v t)$, $U_g = U\sin(\omega_u t)$ and accounting for (18).

3.1 Multiple-scale formulation

The multiple-scale method is employed by introducing four independent timescales, i.e., the fast one, T_0, and the slower ones, T_1, T_2, T_3:

$$T_0 = t, \quad T_1 = \varepsilon t, \quad T_2 = \varepsilon^2 t, \quad T_3 = \varepsilon^3 t \tag{27}$$

where ε is a small dimensionless ordering parameter and, consistently, expressing the time derivatives as

$$\begin{aligned}&\mathrm{d}/\mathrm{d}t = D_0 + \varepsilon D_1 + \varepsilon^2 D_2\\ &\mathrm{d}^2/\mathrm{d}t^2 = D_0^2+2\varepsilon D_0 D_1+\varepsilon^2 D_1^2+2\varepsilon^2 D_0 D_2+2\varepsilon^3 D_1 D_2\end{aligned} \tag{28}$$

where $D_i = \partial/\partial T_i$. Both displacement y and target distance p are scaled as small perturbations of the reference position

$$\begin{aligned} y(t) &= \varepsilon y_1(T_0,T_1,T_2,T_3) + \varepsilon^2 y_2(T_0,T_1,T_2,T_3) \\ &\quad + \varepsilon^3 y_3(T_0,T_1,T_2,T_3) + \varepsilon^4 y_4(T_0,T_1,T_2,T_3) \\ p(t) &= \varepsilon p_1(T_0,T_1,T_2,T_3) + \varepsilon^2 p_2(T_0,T_1,T_2,T_3) \\ &\quad + \varepsilon^3 p_3(T_0,T_1,T_2,T_3) + \varepsilon^4 p_4(T_0,T_1,T_2,T_3) \end{aligned} \tag{29}$$

From Sect. 2.2, the atomic interaction term proves to be directly involved in the definition of the system equilibria, while the other nonlinear terms can be seen as disturbances of these states. Moreover, it is worth noting that typical AFM dimensions and noncontact operating conditions in air and low vacuum have been documented to yield the range of values of dimensionless parameters considered in this analysis (25) ([32,33], details in discussion of Q-factors in [34]). Thus, analyses are restricted to weak damping without considering large damping for operation in water [35] or very small damping for operation in ultrahigh vacuum [36].

Consequently, Γ_1 is set to appear at the generating order, while the other system parameters are rescaled to describe small base excitation amplitude ($V \to \varepsilon^3 \hat{V}$), small scan amplitude ($U \to \varepsilon^3 \hat{U}$), small damping ($\rho_1 \to \varepsilon^2 \hat{\rho}_1$, $\rho_2 \to \varepsilon^2 \hat{\rho}_2$, $\nu_1 \to \varepsilon^2 \hat{\nu}_1$, $\nu_2 \to \varepsilon^2 \hat{\nu}_2$), and small control ($k_g \to \varepsilon^2 \hat{k}_g$). Two detuning terms are also introduced to express the nearness of exciting frequencies to primary resonance

$$\begin{aligned} \varepsilon^2 \sigma_u &= \omega_u - \omega_1 = \omega_1(\Omega_u - 1), \\ \varepsilon^2 \sigma_v &= \omega_v - \omega_1 = \omega_1(\Omega_v - 1) \end{aligned}$$

where ω_1 is the system natural frequency and $\Omega_i = \omega_i/\omega_1$, $i = u, v$.

Note that the feedback control parameter k_g is ordered in such a way to come into play within the perturbation scheme at the same order as the one where the other system nonlinearities appear, i.e., the third order. To evaluate the effect of control on the system asymptotic response, therefore, the perturbation analysis is carried out up to the fourth order.

It is worth underlining here that the reference solution $\tilde{x}_{ref}$ in (26) is the modulated response of the uncontrolled system, and in view of a perturbation analysis, it can be seen as the solution of the perturbed uncontrolled system, which has been obtained, up to the third order, by [6] with the same choice of variables and parameters scaling. Reference is made to the relevant analysis and solution for the sake of comparison: this requires adding here a fourth-order perturbation equation, to ensure that the controlled amplitude becomes directly dependent on the detuning parameter, i.e., to obtain a direct relationship between frequency and amplitude of the controlled response (to be solved numerically), besides indirectly accounting for it via the underlying uncontrolled amplitude.

Hence, $\tilde{x}_{ref}(t)$ can be considered, and thus scaled, as a further variable

$$\begin{aligned} &\tilde{x}_{ref}(t) \\ &= \varepsilon \tilde{x}_{ref1}(T_0,T_1,T_2,T_3) + \varepsilon^2 \tilde{x}_{ref2}(T_0,T_1,T_2,T_3) \\ &\quad + \varepsilon^3 \tilde{x}_{ref3}(T_0,T_1,T_2,T_3) + \varepsilon^4 \tilde{x}_{ref4}(T_0,T_1,T_2,T_3) \end{aligned} \tag{30}$$

For the controlled system, after pre-multiplication by denominator, the following set of perturbation equations is obtained as:

order ε^0 :

$$\Gamma_1 + \bar{x}_{ref}(1+\bar{x}_{ref})^2(\alpha_3 \bar{x}_{ref}^2 + \alpha_1) = 0 \tag{31}$$

order ε^1 :

$$\begin{aligned} &D_0^2 y_1 + \omega_1^2 y_1 + D_0^2 \tilde{x}_{ref1} + \omega_1^2 \tilde{x}_{ref1} + C_{11} p_1 = 0 \\ &D_0 p_1 = 0 \end{aligned} \tag{32}$$

order ε^2 :

$$\begin{aligned} &D_0^2 y_2 + \omega_1^2 y_2 + D_0^2 \tilde{x}_{ref2} + \omega_1^2 \tilde{x}_{ref2} + C_{11} p_2 \\ &\quad = N_{21}(y_1) + N_{22}(\tilde{x}_{ref1}) + N_{23}(p_1) + N_{24}(y_1, \tilde{x}_{ref1}) \\ &\qquad + N_{25}(y_1, p_1) + N_{26}(p_1, \tilde{x}_{ref1}) \\ &D_0 p_2 = -D_1 p_1 \end{aligned} \tag{33}$$

order ε^3 :

$$\begin{aligned} &D_0^2 y_3 + \omega_1^2 y_3 + D_0^2 \tilde{x}_{ref3} + \omega_1^2 \tilde{x}_{ref3} + C_{11} p_3 \\ &\quad = N_{31}(y_1, y_2) + N_{32}(\tilde{x}_{ref1}, \tilde{x}_{ref2}) + N_{33}(p_1, p_2) \\ &\qquad + N_{34}(y_1, y_2, \tilde{x}_{ref1}, \tilde{x}_{ref2}) + N_{35}(y_1, y_2, p_1, p_2) \\ &\qquad + N_{36}(p_1, p_2, \tilde{x}_{ref1}, \tilde{x}_{ref2}) + N_{37}(y_1, \tilde{x}_{ref1}, p_1) \\ &\qquad - C_{cu} \cos(\omega_1 T_0 + \sigma_u T_2 + \phi_u) \\ &\qquad - C_{sv} \sin(\omega_1 T_0 + \sigma_v T_2) \\ &\qquad - C_{su} \sin(\omega_1 T_0 + \sigma_u T_2 + \phi_u) \\ &D_0 p_3 = -D_1 p_2 - D_2 p_1 - \hat{k}_g y_1 \end{aligned} \tag{34}$$

order ε^4 :

$$\begin{aligned} &D_0^2 y_4 + \omega_1^2 y_4 + D_0^2 \tilde{x}_{ref4} + \omega_1^2 \tilde{x}_{ref4} + C_{11} p_4 \\ &\quad = N_{41}(y_1, y_2, y_3) + N_{42}(\tilde{x}_{ref1}, \tilde{x}_{ref2}, \tilde{x}_{ref3}) \\ &\qquad + N_{43}(p_1, p_2, p_3) \\ &\qquad + N_{44}(y_1, y_2, y_3, \tilde{x}_{ref1}, \tilde{x}_{ref2}, \tilde{x}_{ref3}) \end{aligned}$$

$$
\begin{aligned}
&+ N_{45}(y_1, y_2, y_3, p_1, p_2, p_3)\\
&+ N_{46}(p_1, p_2, p_3, \tilde{x}_{ref1}, \tilde{x}_{ref2}, \tilde{x}_{ref3})\\
&+ N_{47}(y_1, y_2, \tilde{x}_{ref1}, \tilde{x}_{ref2}, p_1, p_2)\\
D_0 p_4 &= -D_1 p_3 - D_2 p_2 - D_3 p_1 - \hat{k}_g y_2 \qquad (35)
\end{aligned}
$$

where expressions of C_{ij} coefficients and N_{ij} terms are reported in "Appendix 3" of [37]. It is worth noting that $N_{21}(y_1)$ and $N_{22}(\tilde{x}_{ref1})$ terms have the same structure, as well as $N_{31}(y_1, y_2)$ and $N_{32}(\tilde{x}_{ref1}, \tilde{x}_{ref2})$ terms, $N_{41}(y_1, y_2, y_3)$ and $N_{42}(\tilde{x}_{ref1}, \tilde{x}_{ref2}, \tilde{x}_{ref3})$ terms, $N_{35}(y_1, y_2, p_1, p_2)$ and $N_{36}(\tilde{x}_{ref1}, \tilde{x}_{ref2}, p_1, p_2)$ terms, and $N_{45}(y_1, y_2, y_3, p_1, p_2, p_3)$ and $N_{46}(\tilde{x}_{ref1}, \tilde{x}_{ref2}, \tilde{x}_{ref3}, p_1, p_2, p_3)$ terms. This is due to the fact that the perturbed y and the reference $\tilde{x}_{ref}$ variables appear in all of the terms of (26) simultaneously, apart from some terms related to the forcing V_g, which, in any case, are scaled at higher orders. At each order, furthermore, all the terms of the uncontrolled system can be detected in the controlled system (32)–(35), as functions of $\tilde{x}_{ref}$ and y; the ones related to $\tilde{x}_{ref}$ vanish identically since $\tilde{x}_{ref}$ is the solution for the uncontrolled system. As a consequence, the first equation, at each order, has the same structure as that in [6], apart from replacing $\tilde{x}_{ref}$ with y, including the $\tilde{x}_{ref}\, y$ coupling terms, and exhibiting terms ensuing from the target distance variable p. Hence, neglecting terms related to $\tilde{x}_{ref1}$, solutions of system (32) are

$$
\begin{aligned}
p_1 &= B(T_1, T_2, T_3)\\
y_1 &= A(T_1, T_2, T_3) e^{i\omega_1 T_0}\\
&\quad - C_{11}/\omega_1^2 B(T_1, T_2, T_3) + c.c. \qquad (36)
\end{aligned}
$$

with $A(T_1, T_2, T_3)$ and $B(T_1, T_2, T_3)$ undetermined functions of the slow timescales and $c.c.$ complex conjugate terms (the overbar will denote the complex conjugate and i is the imaginary unit). Solutions (36) highlight that $p_1(T_1, T_2, T_3)$ is a modulated nontrivial equilibrium solution, while $y_1(T_1, T_2, T_3)$ is a harmonic solution modified by the equilibrium position of p_1.

The solution of the perturbation equations up to the fourth order (33)–(35) is reported in "Appendix 2" with the relevant solvability conditions and particular solutions at each order, for both the displacement y and the target distance p.

Once obtained the expressions of $D_j A$, $D_j B$, ($j = 1, 3$) from Eqs. (46), (49), (52), (55), (58), and (61) of "Appendix 2," the usual reconstitution procedure [38] is applied, and the amplitude derivatives with respect to time t are obtained from (28)

$$
\begin{aligned}
\dot{A} &= \varepsilon D_1 A + \varepsilon^2 D_2 A + \varepsilon^3 D_3 A\\
\dot{B} &= \varepsilon D_1 B + \varepsilon^2 D_2 B + \varepsilon^3 D_3 B \qquad (37)
\end{aligned}
$$

The ε parameter is completely reabsorbed through a backward rescaling, and the obtained amplitude modulation equations (AMEs, or bifurcation equations) are (again for the β_i see [37])

$$
\begin{aligned}
\dot{A} &= +\beta_6 AB + \beta_9 A + \beta_5 A_{un} B + \beta_8 B \cos(\sigma_u t + \phi_u)\\
&\quad - \beta_{10} B \sin(\sigma_u t + \phi_u) + \beta_{11} B \cos(\sigma_v t)\\
&\quad + i\left(\bar{A}_{un}\left(A^2(\beta_1 B + \beta_4) + 2AA_{un}(\beta_1 B + \beta_4)\right.\right.\\
&\quad \left.\left. + \beta_1 A_{un}^2 B\right) + A^2 \bar{A}(\beta_1 B + \beta_4) + 2\beta_4 A \bar{A} A_{un}\right.\\
&\quad + AB\left(2\beta_1 \bar{A} A_{un} + B(\beta_2 B + \beta_3) + \beta_7\right)\\
&\quad + A_{un}\left(B\left(\beta_1 \bar{A} A_{un} + B(\beta_2 B + \beta_3) + \beta_7\right)\right.\\
&\quad \left. + \beta_4 \bar{A} A_{un}\right) + B(\beta_8 \sin(\sigma_u t + \phi_u)\\
&\quad + \beta_{10} \cos(\sigma_u t + \phi_u) + \beta_{11} \sin(\sigma_v t)))\\
\dot{B} &= \frac{2C_{214} k_g}{\omega_1^2}\left(A\bar{A}_{un} + A\bar{A} + \bar{A} A_{un}\right)\\
&\quad + \frac{C_{212} k_g}{\omega_1^2} B^2 + \frac{C_{11} k_g}{\omega_1^2} B \qquad (38)
\end{aligned}
$$

Note that the complex amplitudes A and B are of order ε ($A = \varepsilon A$, $B = \varepsilon B$), as they refer to the displacement y and the target distance p, respectively.

To write the system (38) in Cartesian coordinates, it has to be transformed in an autonomous form, so the presence of resonant external vertical excitation V_g or resonant parametric horizontal excitation U_g has to be taken into account separately. For the horizontally forced case ($V_g = 0$), by means of the coordinates transformations,

$$
\begin{aligned}
A &= \frac{1}{2}(j(t) + i\, n(t)),\\
\bar{A} &= \frac{1}{2}(j(t) - i\, n(t)), \quad B = b(t),\\
A_{un} &= \frac{1}{2}(j_{un}(t) + i\, n_{un}(t)),\\
\bar{A}_{un} &= \frac{1}{2}(j_{un}(t) - i\, n_{un}(t))
\end{aligned}
$$

system (38) results in

$$
\begin{aligned}
\dot{j}(t) &= -\beta_2 n(t) b(t)^3 - \beta_2 n_{un}(t) b(t)^3 - \beta_3 n(t) b(t)^2\\
&\quad - \beta_3 n_{un}(t) b(t)^2 - \frac{\beta_1}{4} j_{un}(t)^2 n_{un}(t) b(t)\\
&\quad - \frac{\beta_1}{4} n_{un}(t)^3 b(t) + \beta_5 j_{un}(t) b(t) + \beta_6 j(t) b(t)\\
&\quad - \beta_7 n(t) b(t) - \beta_7 n_{un}(t) b(t) + 2\beta_8 b(t)
\end{aligned}
$$

$$
\begin{aligned}
&- \frac{\beta_1}{4} j(t)^2 n_{un}(t) b(t) - \frac{3\beta_1}{4} n(t)^2 n_{un}(t) b(t) \\
&- \frac{\beta_1}{2} j(t) j_{un}(t) n(t) b(t) - \frac{\beta_1}{4} j_{un}(t)^2 n(t) b(t) \\
&- \frac{3\beta_1}{4} n(t) n_{un}(t)^2 b(t) - \frac{\beta_1}{4} j(t)^2 n(t) b(t) \\
&- \frac{\beta_1}{2} j(t) j_{un}(t) n_{un}(t) b(t) \\
&- \frac{\beta_1}{4} n(t)^3 b(t) + \beta_9 j(t) - \frac{\beta_4}{4} j(t)^2 n_{un}(t) \\
&- \frac{\beta_4}{4} j_{un}(t)^2 n(t) - 3\frac{\beta_4}{4} n(t)^2 n_{un}(t) \\
&- 3\frac{\beta_4}{4} n(t) n_{un}(t)^2 - \frac{\beta_4}{4} j(t)^2 n(t) \\
&- \frac{\beta_4}{2} j(t) j_{un}(t) n(t) - \frac{\beta_4}{2} j(t) j_{un}(t) n_{un}(t) \\
&- \frac{\beta_4}{4} n(t)^3 + (\omega_1 \Omega_u - \omega_1) n(t) \qquad (39)
\end{aligned}
$$

$$
\begin{aligned}
\dot{n}(t) = {} & \beta_2 j(t) b(t)^3 + \beta_2 j_{un}(t) b(t)^3 + \beta_3 j(t) b(t)^2 \\
&+ \beta_3 j_{un}(t) b(t)^2 + \frac{\beta_1}{4} j_{un}(t)^3 b(t) \\
&+ \frac{\beta_1}{4} j_{un}(t) n_{un}(t)^2 b(t) + \beta_5 n_{un}(t) b(t) \\
&+ \beta_6 n(t) b(t) + \beta_7 j(t) b(t) \\
&+ \beta_7 j_{un}(t) b(t) + 2\beta_{10} b(t) \\
&+ 3\frac{\beta_1}{4} j(t)^2 j_{un}(t) b(t) + \frac{\beta_1}{4} j_{un}(t) n(t)^2 b(t) \\
&+ \frac{\beta_1}{2} j(t) n(t) n_{un}(t) b(t) + 3\frac{\beta_1}{4} j(t) j_{un}(t)^2 b(t) \\
&+ \frac{\beta_1}{4} j(t) n_{un}(t)^2 b(t) + \frac{\beta_1}{4} j(t)^3 b(t) \\
&+ \frac{\beta_1}{4} j(t) n(t)^2 b(t) + \frac{\beta_1}{2} j_{un}(t) n(t) n_{un}(t) b(t) \\
&+ \beta_9 n + 3\frac{\beta_4}{4} j(t)^2 j_{un}(t) + 3\frac{\beta_4}{4} j(t) j_{un}(t)^2 \\
&+ \frac{\beta_4}{4} j(t) n_{un}(t)^2 + \frac{\beta_4}{4} j_{un}(t) n(t)^2 \\
&+ \frac{\beta_4}{4} j(t)^3 + \frac{\beta_4}{4} j(t) n(t)^2 + \frac{\beta_4}{2} j(t) n(t) n_{un}(t) \\
&+ \frac{\beta_4}{2} j_{un}(t) n(t) n_{un}(t) + (\omega_1 - \omega_1 \Omega_u) j(t)
\end{aligned}
$$

$$
\begin{aligned}
\dot{b}(t) = {} & \frac{C_{212} k_g}{\omega_1^2} b(t)^2 + \frac{C_{11} k_g}{\omega_1^2} b(t) + \frac{C_{214} k_g}{2\omega_1^2} j(t)^2 \\
&+ \frac{C_{214} k_g}{\omega_1^2} j(t) j_{un}(t) + \frac{C_{214} k_g}{2\omega_1^2} n(t)^2 \\
&+ \frac{C_{214} k_g}{\omega_1^2} n(t) n_{un}(t)
\end{aligned}
$$

where $j(t)$ and $n(t)$ are the real and imaginary parts of the complex amplitude A, respectively, and $j_{un}(t)$ and $n_{un}(t)$ are the real and imaginary parts of the reference complex amplitude A_{un}, respectively.

The asymptotic system is completed by the perturbation equations furnished by the analysis of the uncontrolled system, for which the solvability condition at the fourth order implies that $D_3 A_{un} = 0$, thus not modifying the amplitude equations obtained in [6]. In Cartesian coordinates, they result

$$
\begin{aligned}
\dot{j}_{un}(t) = {} & + \frac{C_{su}}{2\omega_1} - \frac{C_{35}}{2} j_{un}(t) + n_{un}(t)\omega_1 (\Omega_u - 1) \\
&- \frac{C_{301}}{8\omega_1} \left(j_{un}(t)^2 n_{un}(t) + n_{un}(t)^3 \right) \\
\dot{n}_{un}(t) = {} & + \frac{C_{cu}}{2\omega_1} - \frac{C_{35}}{2} n_{un}(t) - j_{un}(t)\omega_1 (\Omega_u - 1) \\
&+ \frac{C_{301}}{8\omega_1} \left(n_{un}(t)^2 j_{un}(t) + j_{un}(t)^3 \right) \qquad (40)
\end{aligned}
$$

Similar equations are obtained in the vertically forced case.

Finally, the expression of the asymptotic solution of (26) is obtained by remembering that it has been proposed as a series expansion of y (29). Thus, contributions up to the third order can be reconstituted by making use of (36), (47), (50), (53), (56), and applying a backward rescaling and the transformation to Cartesian coordinates. The steady-state responses result

$$
\begin{aligned}
y = {} & f_{y0} + f_{yc1} \cos(\omega_1 t) + f_{ys1} \sin(\omega_1 t) \\
&+ f_{yc2} \cos(2\omega_1 t) + f_{ys2} \sin(2\omega_1 t) \\
&+ f_{yc3} \cos(3\omega_1 t) + f_{ys3} \sin(3\omega_1 t) \\
p = {} & f_{p0} + f_{pc1} \cos(\omega_1 t) + f_{ps1} \sin(\omega_1 t) \qquad (41)
\end{aligned}
$$

where coefficients f_{hkl} are reported in "Appendix 4."

3.2 Stability analysis

To analyze the stability of the asymptotic solution, the Jacobian matrix of the complete system ((39) and (40)) at the desired dynamic equilibrium $\mathbf{a_e} = (j_{un}, n_{un}, j, n, b)$ is studied, as done previously in Sect. 2.2 for the system fixed points

$$
\mathbf{J}_{\mathbf{a_e}} = \begin{bmatrix}
c_{11} & c_{12} & c_{13} & c_{14} & c_{15} \\
c_{21} & c_{22} & c_{23} & c_{24} & c_{25} \\
c_{31} & c_{32} & c_{33} & c_{34} & c_{35} \\
c_{41} & c_{42} & 0 & 0 & 0 \\
c_{51} & c_{52} & 0 & 0 & 0
\end{bmatrix} \qquad (42)
$$

where the terms c_{hk}, $h,k = 1,...,5$ of the Jacobian matrix are reported in "Appendix 3." Note that when the system response settles to the reference one, i.e., $j = n = b = 0$, the controlled problem (which corresponds to the first three lines of (42)) and the uncontrolled one (last two lines of (42)) are decoupled, so the Routh–Hurwitz stability criterion can be applied only to the controlled part. Thus, the stability analysis is reduced to the study of the coefficients of the characteristic polynomial $p_{\mathbf{J_{ae}}}(\lambda) = \lambda^3 + P_1\lambda^2 + P_2\lambda + P_3 = 0$ where

$$\begin{aligned} P_1 &= -\mathrm{tr}\,(p) = -c_{13} - c_{24} - c_{35} \\ P_2 &= \mathrm{Z}\,(p) = -c_{14}c_{23} - c_{15}c_{33} - c_{25}c_{34} + c_{24}c_{35} \\ &\quad + c_{13}c_{24} + c_{13}c_{35} \\ P_3 &= -\det\,(p) = c_{15}\,(c_{24}c_{33} - c_{23}c_{34}) \\ &\quad + c_{14}\,(c_{23}c_{35} - c_{25}c_{33}) \\ &\quad + c_{13}\,(c_{25}c_{34} - c_{24}c_{35}) \\ \Delta_2 &= P_1P_2 - P_3 \end{aligned} \tag{43}$$

The asymptotic stability is guaranteed if and only if

$$\begin{cases} P_i > 0, \quad i = 1,2,3 \\ \Delta_2 > 0 \end{cases} \tag{44}$$

However, note that the coefficients in (43) incorporate a complex implicit parameter description for the equilibrium position as ensuing from the solution of Eq. (40). In light of this, in the following section, the stability of the asymptotic system will be investigated by numerically solving the five equation system, so as to simultaneously obtain the controlled and the reference amplitudes.

4 Validity of the asymptotic solution and effectiveness of control

To check the validity of the asymptotic solution, AMEs of the uncontrolled system (40) are added to the controlled ones (39). Denoting with $a = \sqrt{j^2 + n^2}$ and $a_{un} = \sqrt{j_{un}^2 + n_{un}^2}$, the amplitudes of the trivial solution $(a,b) = (0,0)$ of the controlled system and of the uncontrolled one, respectively, Fig. 4 highlights the effectiveness of the control technique in setting the system response to the reference one, besides furnishing the asymptotic approximation of the latter.

Once verified the effectiveness of control as furnished by the asymptotic solution, an additional check is developed comparing the asymptotic solution—as obtained with the enlarged (i.e., controlled) system—with the results obtained via numerical integration of the system Eq. (16), for the vertically and horizontally forced system, separately. Note that to properly compare the stationary responses of the asymptotic Eqs. (39) and (40) with the ones obtained from the ordinary differential system (16), the definition of the asymptotic variables has to be recalled, to obtain $x = y + \bar{x}_{ref} + \tilde{x}_{ref}$ and $z = p + z_s$. Here, y and p are the controlled solutions reported in (41), $\bar{x}_{ref}$ and z_s are the system equilibrium positions obtained in Sect. 2.2, and $\tilde{x}_{ref}$ is the time-dependent part of the reconstituted reference solution. Similarly, when comparing the asymptotic and numerical amplitudes, the first one is furnished by the sum of the controlled amplitude a (obtained from system (39)) and the reference amplitude a_{un} (obtained from system (40)), while the latter is evaluated from $(x_{max} - x_{min})/2$. For what concerns the control variable z, the numerical results have to be manipulated by

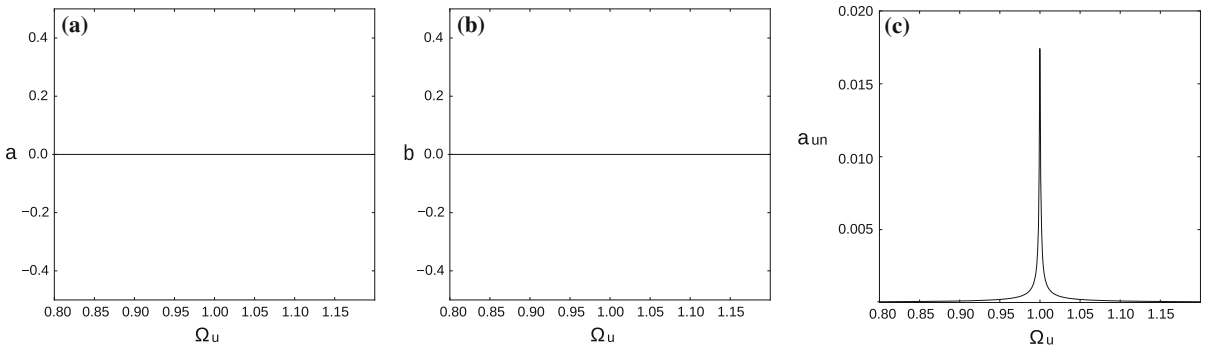

Fig. 4 Asymptotic solutions for the parametrically forced system at $U_g = 0.0001$ and $k_g = 0.001$: controlled amplitudes a, b (**a**) and uncontrolled amplitude a_{un} (**b**)

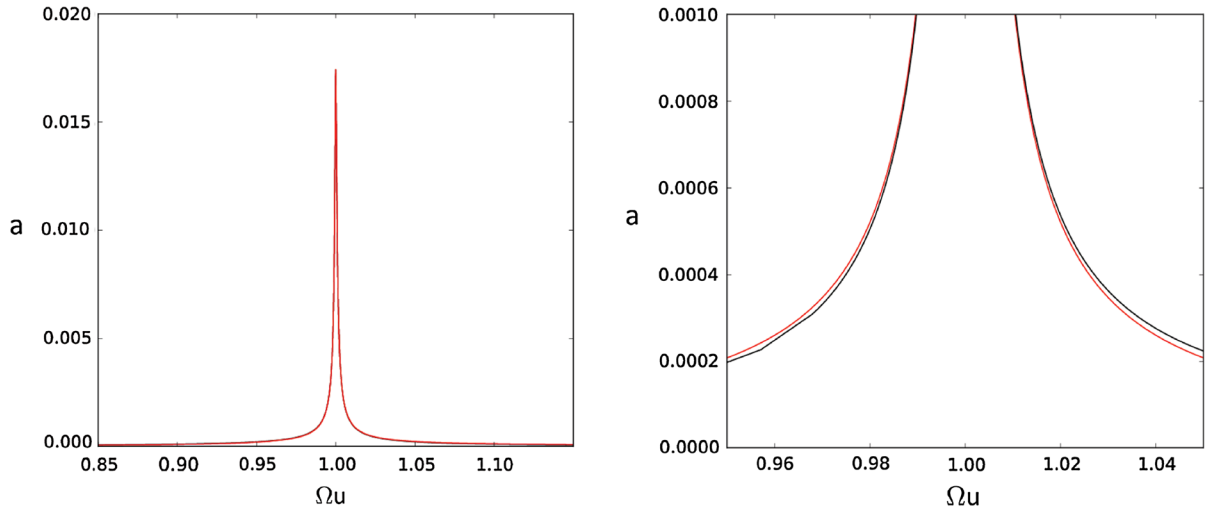

Fig. 5 Frequency–response curve: asymptotic (*red line*) and numerical (*black line*) solutions for the parametrically forced system at $U_g = 0.0001$ and $k_g = 0.001$. (Color figure online)

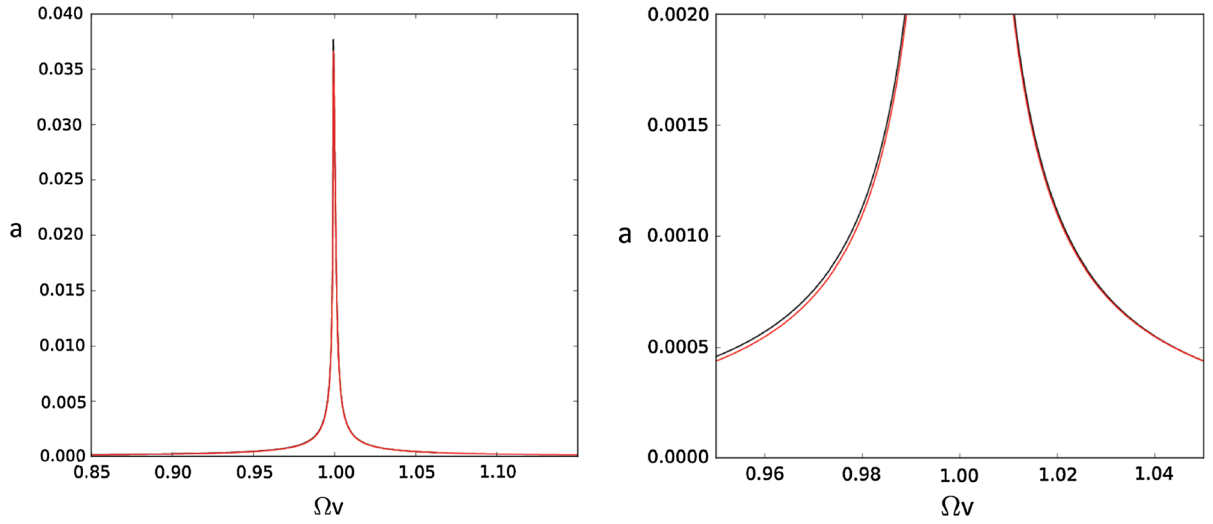

Fig. 6 Frequency–response curve: asymptotic (*red line*) and numerical (*black line*) solutions for the externally forced system at $V_g = 0.0001$ and $k_g = 0.001$. (Color figure online)

evaluating the mean value $(z_{max} + z_{min})/2$, due to the fact that the asymptotic amplitude b represents the correction to the equilibrium position z_s (the generating solution of b is constant, while the one corresponding to the a amplitude is oscillating, see (36)).

4.1 Frequency–response curves

Figures 5, 6 are obtained for $k_g = 0.001$ and demonstrate that the asymptotic solutions (red lines) are in very good agreement with the behavior of the original ODEs (black lines). It is interesting to point out that the amplitude of the system response under horizontal excitation is half the one obtained with the vertical force; this is due to the fact that the primary resonance is the most relevant one for an externally driven system, while the parametric excitation affects mainly the order $-1/2$ subharmonic resonance.

Figure 7a confirms the good concordance of results by the comparison between frequency–response curves obtained for the AMEs and for the ODEs at a feed-

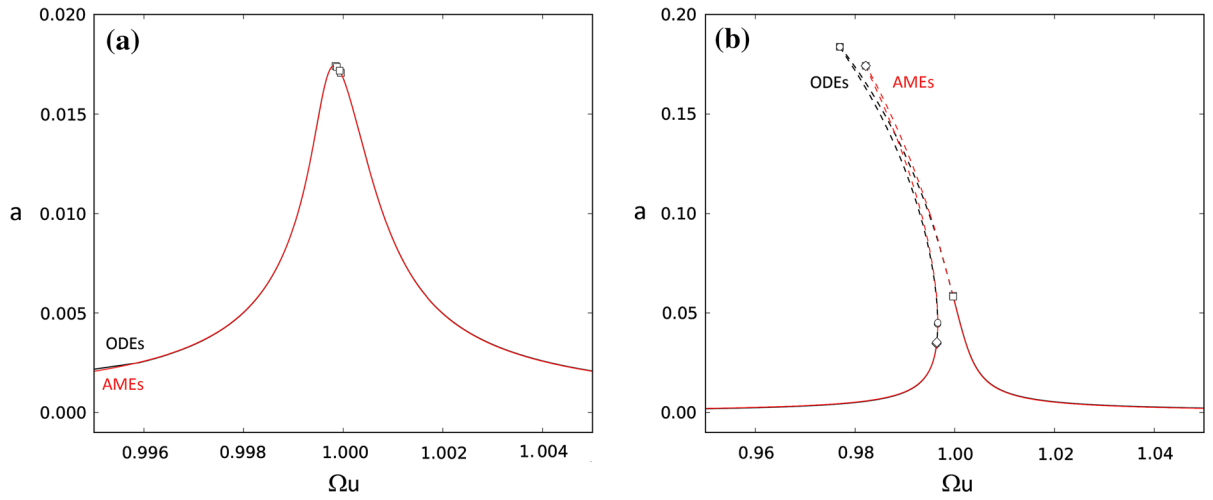

Fig. 7 Comparison between results obtained from ODEs system (*black*) and from AMEs system (*red*) for $U = 0.0001$ and $k_g = 0.002$ (**a**) and for $U = 0.001$ and $k_g = 0.001$ (**b**). (Color figure online)

back control value close to the limit value $k_g = 0.002$ (see Sect. 2.2). The reported curves almost overlap, as well as the very narrow region of instability confined by a couple of transcritical bifurcations, underlining the capability of the asymptotic system to grasp the changes in the response stability.

Also for an increased forcing amplitude value $U = 0.001$ (Fig. 7b), the asymptotic system provides good results, even if slight differences occur around the top of the resonance curve, where the high value of the response amplitude does not fulfill the ordering of the asymptotic system (i.e., $a = \varepsilon a$).

4.2 Bifurcation structure

A more systematic analysis of the accuracy of the asymptotic solution in terms of response and its stability is made by looking at the bifurcation behavior with varying system parameters. First, the effect of the feedback control parameter is analyzed, by referring to the horizontally forced system. The behavior chart in Fig. 8a shows the stability threshold of the bounded reference solution. The results show that the asymptotic system loses its stability through a Hopf bifurcation, except for a confined region around the resonance peak, for which instability arises via a transcritical bifurcation (see frequency–response curve of Fig. 7a). It is evident the similarity between the qualitative behavior of the analyzed system and the same results obtained for the original system of ODEs reported in Fig. 8b, just considering that a torus bifurcation of a periodic solution corresponds to a Hopf bifurcation of the relevant amplitude asymptotic solution. The good agreement of the results concerns also the quantitative aspect, as shown in Fig. 8c, with an error on the amplitude of about 2 %. Note that, away from nearly perfect resonance, the k_g limit value corresponding to the Hopf (Torus) bifurcation is the same as the one obtained studying the asymptotic stability of the equilibrium solution in Sect. 2.2 (i.e. $k_g = 0.00223$).

To further confirm the accuracy of the asymptotic approximation, while at the same time getting hints on the variety of system regular and nonregular responses, additional bifurcation diagrams, for increasing values of the feedback control parameter k_g and of the forcing amplitude U, are reported in Figs. 9, 12, together with the corresponding results obtained for the original ODEs, along with some sample response (Figs. 10, 11, 13).

The evolution of the asymptotic response in terms of maximum displacement (left) and target distance (right) amplitudes, as a function of k_g, is reported in Fig. 9a at a forcing frequency value close to the primary resonance $\Omega_u = 0.9999$; comparison has to be made with the ODEs results (Fig. 9b). Both the asymptotic system and the original one exhibit the presence of a main periodic solution P1 which is present also in the uncontrolled case (i.e., for $k_g = 0$) and which is properly controlled by the system (the control vari-

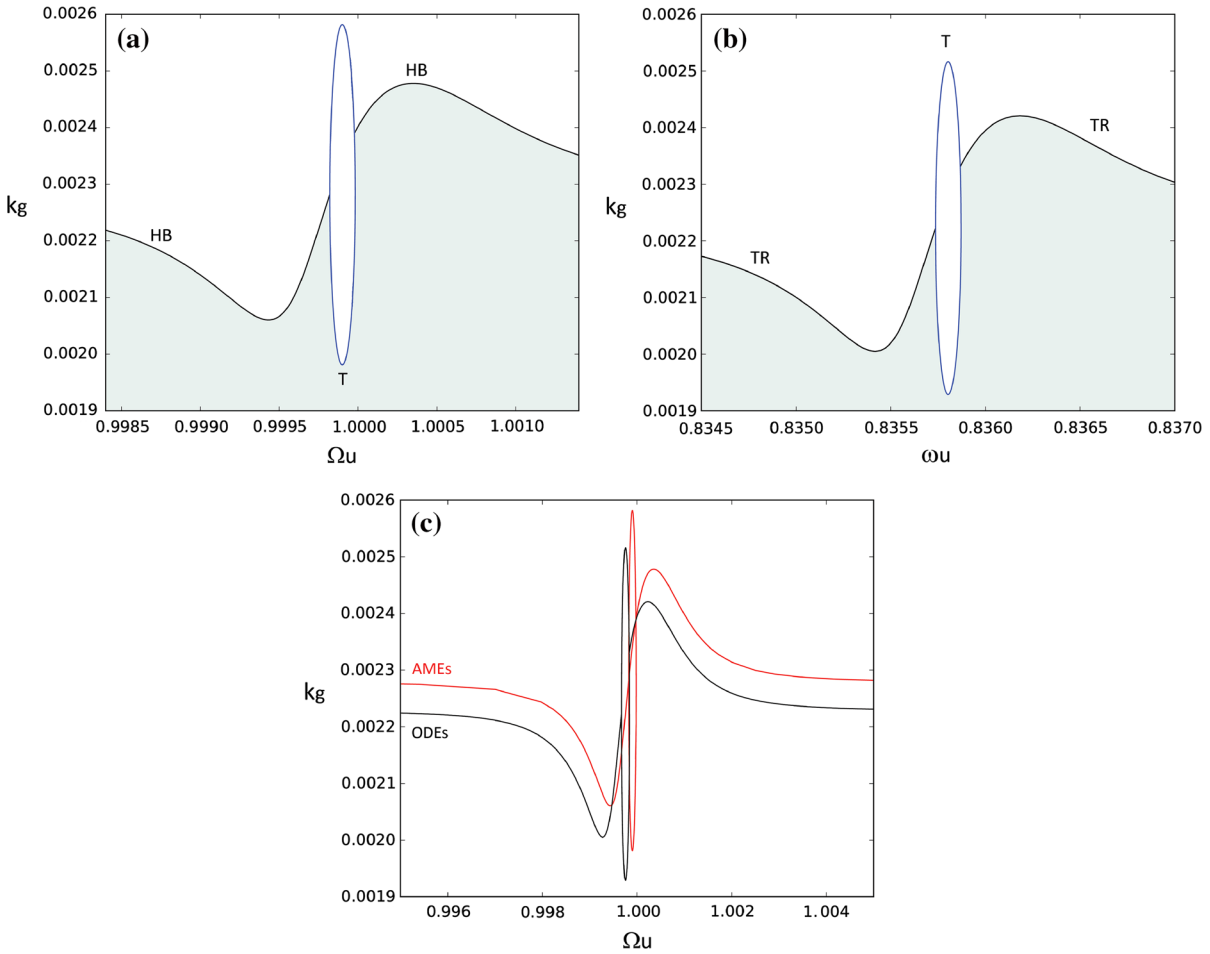

Fig. 8 Behavior charts in the Ω_u-k_g (ω_u-k_g) plane around primary resonance at $U = 0.0001$ for the asymptotic system (**a**) and for the original ODEs system (**b**). Comparison between asymptotic (*red curve*) and original system (*black curve*) results (**c**). TR: torus bifurcation, HB: Hopf bifurcation, T: transcritical bifurcation, *gray region*: stable region (bounded reference solution). (Color figure online)

able z, with amplitude b, settles to the desired position $z_s = 0.01$, see also Fig. 10). At $k_g = 0.00193$, a transcritical bifurcation T makes such solution unstable and brings to the arise of two periodic solutions P1′ and P1″ which are typical of the controlled system while do not exist in the uncontrolled reference one, and for which the control variable z does not reach the expected position z_s (see the right side of Fig. 9a, b). Yet, even if they do not represent the goal of the control procedure, also in this case, an excellent agreement between the results of the two systems is observed, not only about the qualitative behavior of the response but also about the detection of the bifurcation events responsible for changes in stability. Moreover, in order to complete the description of the system responses, phase portraits and Poincaré maps of the three 1-period solutions obtained from the numerical system (16) (black) and from the steady-state responses (41) of the asymptotic system (red) are compared in Figs. 10 and 11. As regards the P1 solution, Fig. 10 shows the overlapping of the results and confirms the ability of the control procedure in setting the response at the reference value z_s, while for the new P1′ and P1″ solutions, Fig. 11 highlights that the concordance between numerical and asymptotic results is affected by the increased value of the feedback control parameter k_g and by the transition of the z variable from a constant to a periodic behavior. However, the outcomes reveal satisfactory results also from a quantitative viewpoint, just considering the figures scale.

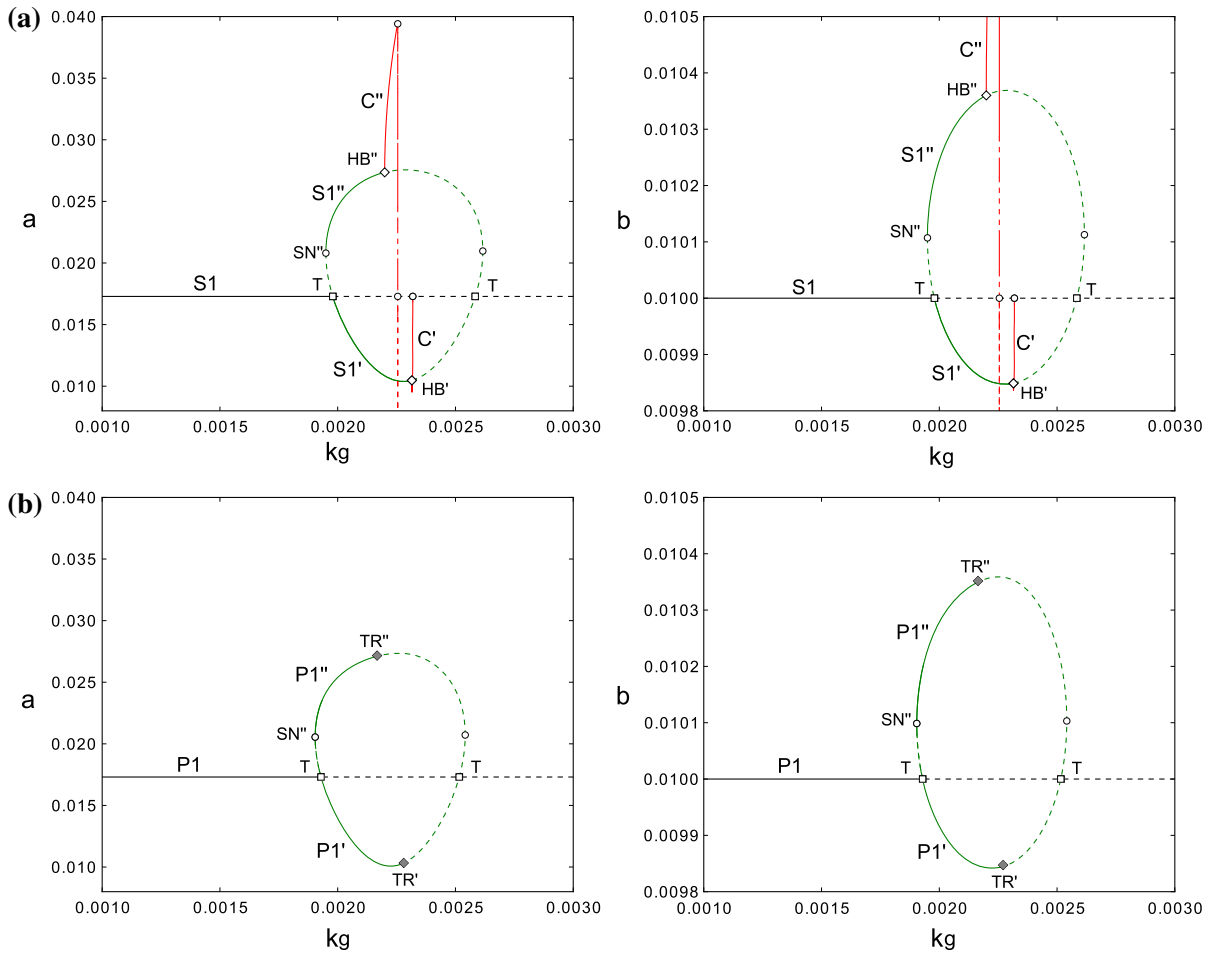

Fig. 9 Bifurcation diagram at $U = 0.0001$ for varying k_g at $\Omega_u = 0.9999$ for the asymptotic system (**a**) and at $\omega_u = 0.8358$ (corresponding to $\Omega_u = 1$) for the ODEs system (**b**). S1,S1',S1": equilibrium solutions in the AMEs which correspond to P1,P1',P1" periodic solutions in the ODEs; C',C": limit cycles in the AMEs which correspond to quasiperiodic solutions in the ODEs; HB: Hopf bifurcation in the AMEs which correspond to torus bifurcation (TR) in the ODEs; T: transcritical bifurcation; SN: saddle-node bifurcation. (Color figure online)

Furthermore, power spectra in Figs. 10 and 11 show that the reported 1-period solutions are dominated by the forcing frequency ($f_1 = \omega_u/2\pi \cong 0.133$), with also the presence of its superharmonics ($f_2 = \omega_u/\pi \cong 0.266$ and $f_3 = 3\omega_u/2\pi \cong 0.399$). Note that the results obtained for the asymptotic responses (red lines) are able to depict the presence of the superharmonics peaks in the x variable, while can detect only the dominating peak in the z variable, as it was reasonable to expect by looking at their expressions (41) where the contributions of the double and triple frequencies are present only in the x case.

To analyze the validity of the asymptotic response as a function of the forcing amplitude, bifurcation diagrams for increasing U are reported in Fig. 12 at a forcing frequency $\omega_u = 0.82$ (corresponding to $\Omega_u = 0.98$). It is worth underlining here that the asymptotic system allows one to select and follow also the evolution of the original system quasiperiodic responses, which appear as periodic solutions arisen from the Hopf bifurcations (red curves C in Fig. 12 and C$'$ and C$''$ in Fig. 9a). This is the case, for example, of the quasiperiodic solution of Fig. 13, for an amplitude value of $\cong 0.012$; the time series obtained from the ordinary differential system (16) reported in Fig. 13a depict quasiperiodic beats with a long period $T = 651.5$ that corresponds to a frequency $f = 0.0015$, detected in the power spectra of Fig. 13c very close to the zero

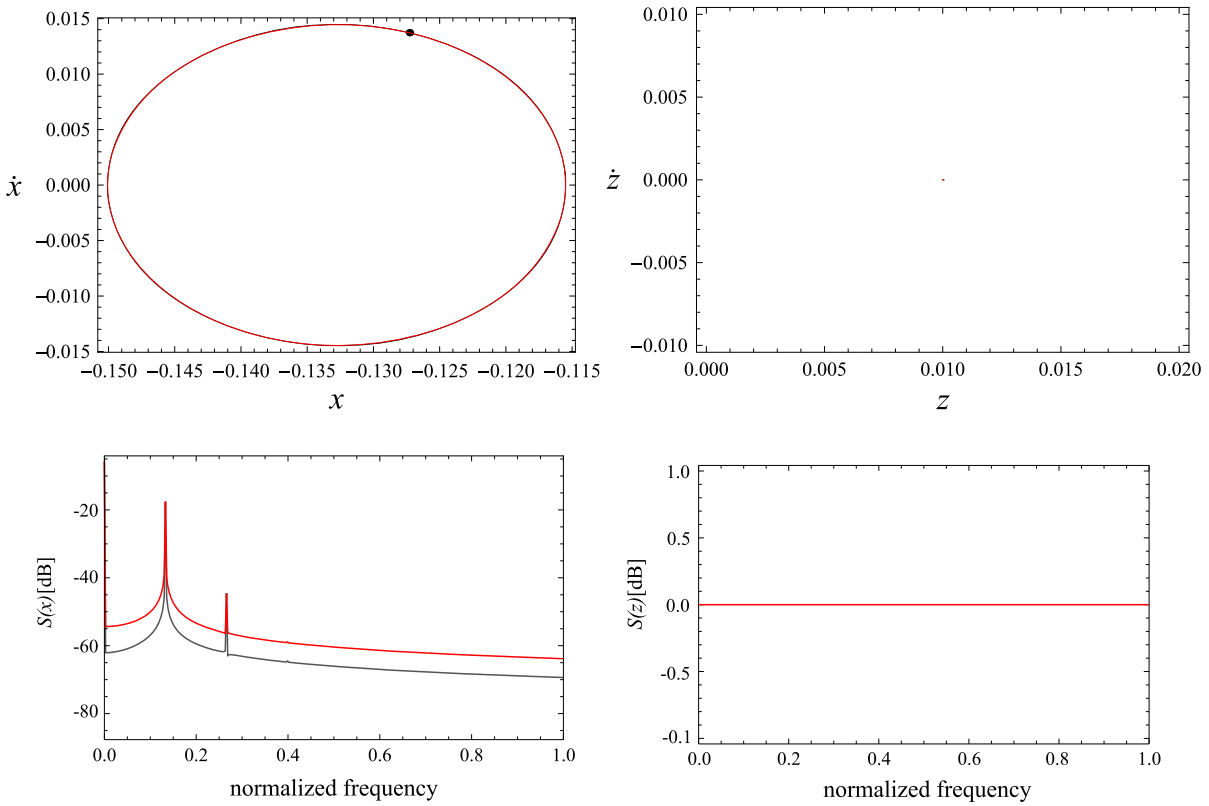

Fig. 10 Comparison between asymptotic (*red*) and numerical (*black*) responses at fundamental resonance for the P1 (S1) solution at $k_g = 0.0015$. (Color figure online)

value. Even for these solutions, the asymptotic system response, represented by the red graphics of Fig. 13b, c, proves to be able to properly reproduce the system behavior, both from a qualitative and a quantitative viewpoint.

As a final remark, it is worth noting that the results reported in Fig. 8 are qualitatively similar to those presented by [23], obtained for a simple model of tapping AFM subject to the same external feedback control technique and operating in the noncontact region. Figures 7 and 10 of [23], in fact, show the stability thresholds of the externally forced system around primary resonance, obtained from the approximate averaged system and from numerical computations, respectively. The present detection of the transcritical and Hopf bifurcation thresholds for both the horizontal and the vertical excitation (latter results not reported) confirms the goodness of the obtained outcomes and allows one to reasonably assume that the described behavior is typical of AFM systems in noncontact regime under the presented kind of feedback control and irrespective of the considered resonant (parametric or external) excitation.

5 Closing remarks

An external feedback control has been introduced into the continuum formulation of a noncontact AFM microcantilever, with the aim of avoiding possible unstable motions of the system. The control consists of maintaining the microcantilever vibration close to the reference one which corresponds to an operationally suitable response obtained for the uncontrolled system with the same set of parameter values. Accordingly, the uncontrolled system proposed by [6] has been enriched by the addition of a new variable in the distributed parameter system equations. This variable represents the distance between the microcantilever fixed boundary and the horizontal reference axis and modifies the terms dependent on the tip-sample distance, i.e., the nonlinear atomic interaction term and the vertical boundary con-

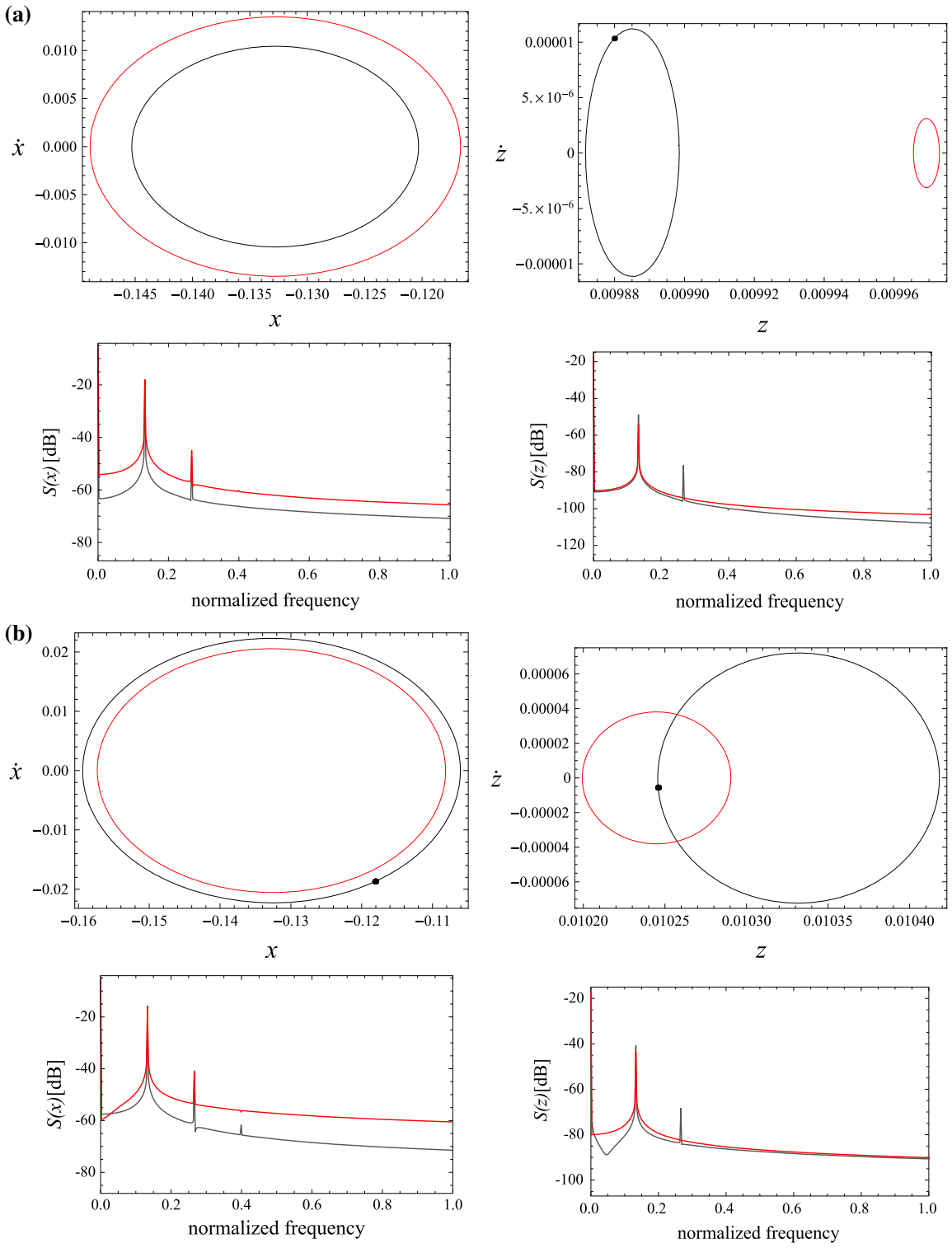

Fig. 11 Comparison between asymptotic (*red*) and numerical (*black*) responses at fundamental resonance: P1′ (S1′) solution (**a**) and P1″ (S1″) solution (**b**) at $k_g = 0.002$. (Color figure online)

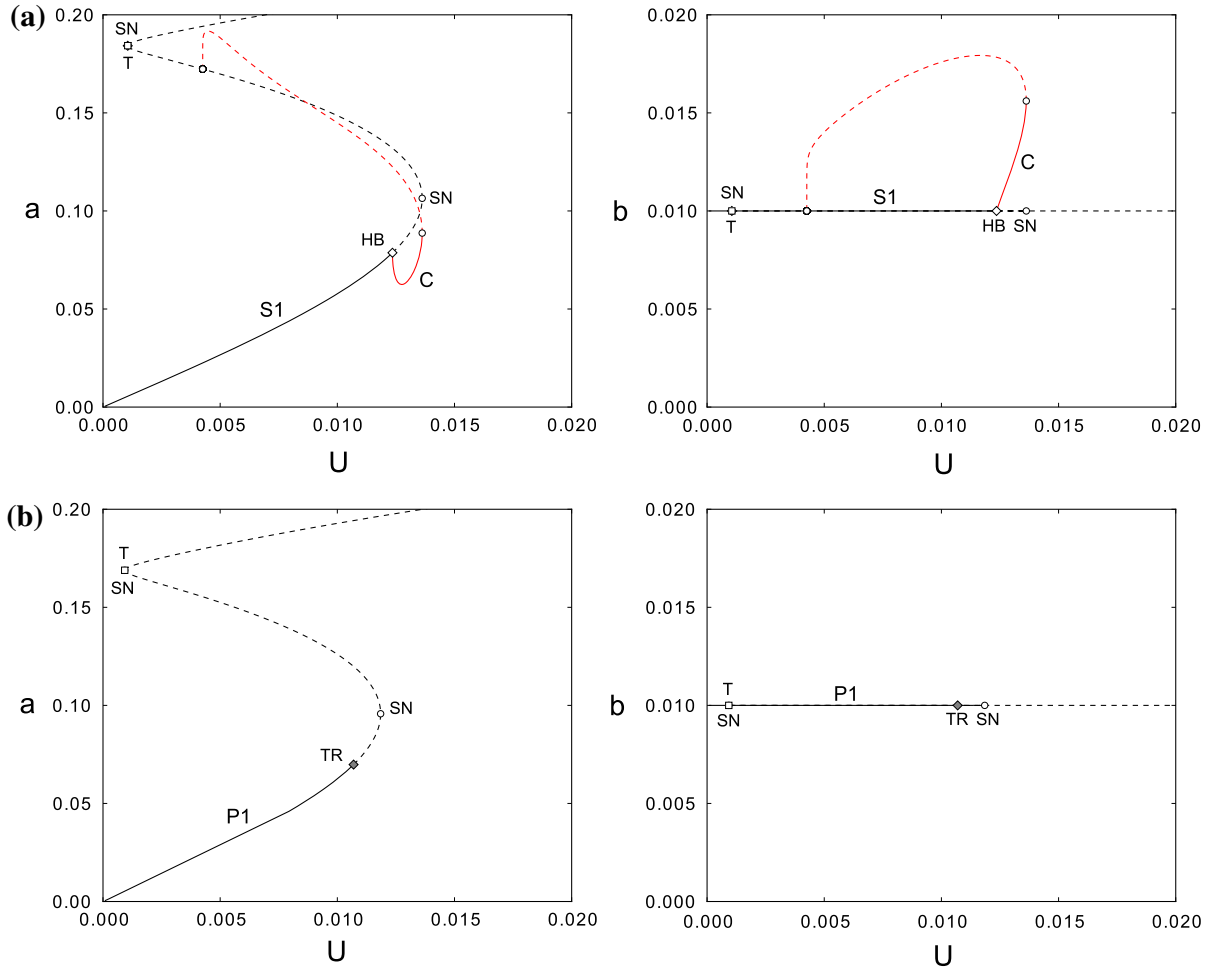

Fig. 12 Bifurcation diagram at $k_g = 0.001$ for varying U at $\Omega_u = 0.98$ (corresponding to $\omega_u = 0.82$) for the asymptotic system (**a**) and for the ODEs system (**b**). S1: equilibrium solution in the AMEs which correspond to P1 periodic solutions in the ODEs; C: limit cycle in the AMEs which correspond to quasiperiodic solutions in the ODEs; HB: Hopf bifurcation in the AMEs which correspond to torus bifurcation (TR) in the ODEs; T: transcritical bifurcation; SN: saddle-node bifurcation. (Color figure online)

ditions. A single-mode reduction based on the Galerkin procedure has been implemented to obtain the equations of motion governing the dynamics of the controlled model.

The equilibrium analysis reveals that the control does not affect the existence of equilibrium states but significantly influences their stability by a substantial reduction in the stable range due to the presence of a new threshold for a Hopf bifurcation.

The validation of the applied feedback control technique and the investigation of the nonlinear dynamics around the desired fixed point close to primary resonance have been carried out by means of the method of multiple scales, which yields a reduced set of evolution equations that approximate the slow-time amplitudes of motion. A very good correspondence between asymptotic prediction and system response obtained via numerical integration, also for quite high values of the most relevant system parameters, demonstrates the effectiveness of the control technique in setting the system response to the reference one. This confirms that the control method represents a simple and efficient procedure for reliable AFM sample surface measurement in the weakly nonlinear dynamic regime.

Furthermore, system parameters stability maps and bifurcation diagrams depicting response amplitude as a function of the feedback control parameter k_g demonstrate the quantitative accuracy of the asymp-

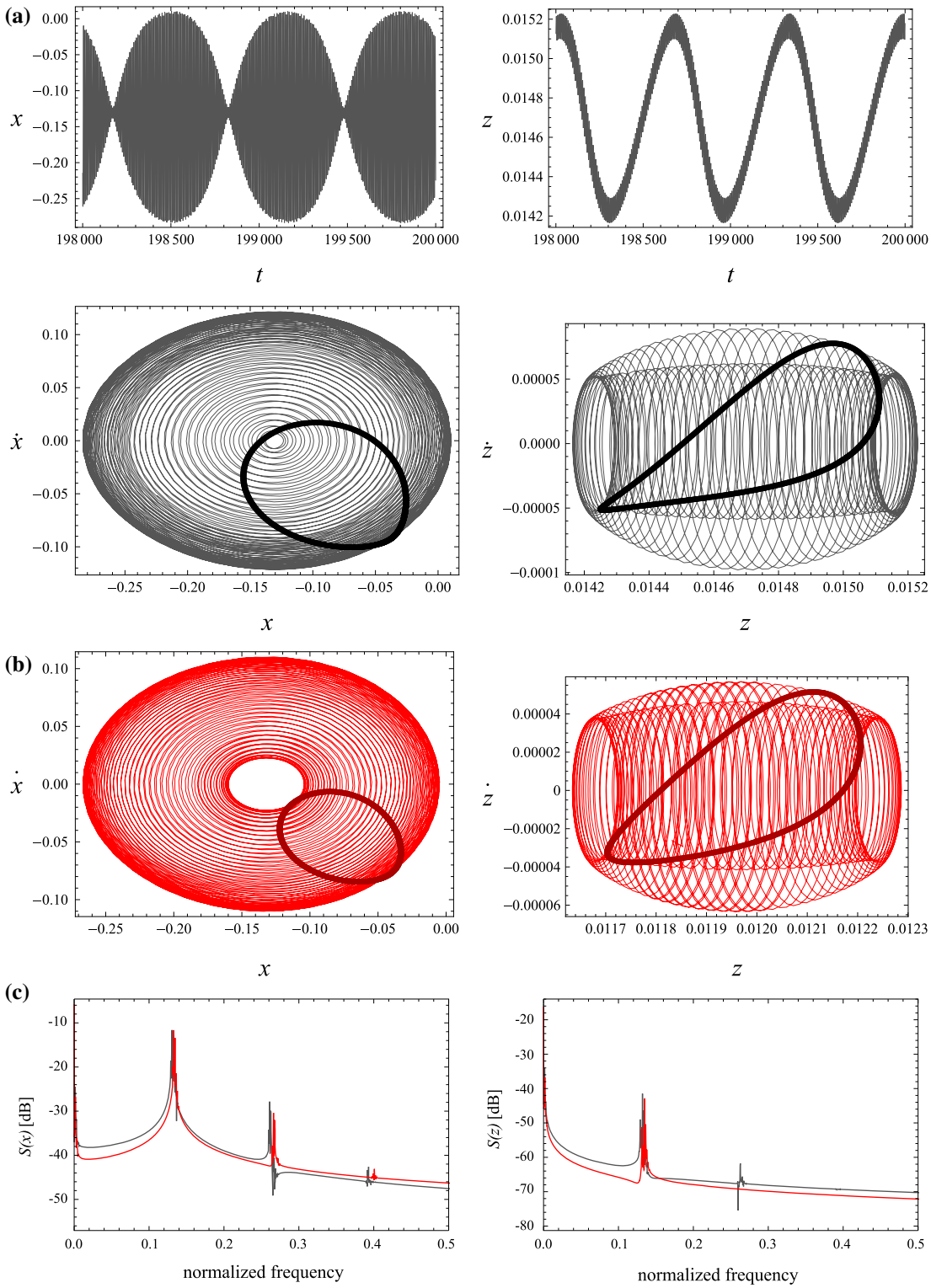

Fig. 13 Quasiperiodic solutions at $\omega_u = 0.82$ ($\cong \Omega_u = 0.98$) and $U \cong 0.012$ obtained from the numerical system (**a**) and from the asymptotic system (**b**), and comparison between the relevant power spectra (**c**). (Color figure online)

totic solutions and highlight novel peculiarities of system response, such as an enriched bifurcation scenario characterized by the existence of transcritical and torus bifurcations culminating with the onset of additional periodic solutions and quasiperiodic solutions, respectively.

In a more general perspective, the proposed model, although entailing a strong simplification of the various and complex phenomena that are known to characterize the AFM operation and that can be investigated only via experimental analyses, proved to be able to grasp the fundamental aspects of the system itself and, at the same time, to be sufficiently manageable to be treated with both analytical and numerical methods. In this spirit, it is useful to investigate the system stability and identify the safe and unsafe regions depending on its main parameters, thus also providing guidance on those behaviors that experimentalists can expect to find. Moreover, the results obtained with this model also provide information on the effects of a local control on the overall dynamical behavior of the system and then allow one to more generally evaluate the effectiveness and possible criticalities of a category of control techniques.

Acknowledgments Oded Gottlieb acknowledges the partial support of the Israel Science (1475/09) and Giuseppe Rega acknowledges the partial support of the Sapienza University of Rome (C26A12R2L2). Valeria Settimi is grateful to the Sapienza University of Rome for the financial support via a post doc scholarship and to the Russell Berrie Nanotechnology Institute for support of her stay at the Technion.

Appendix 1

The integral expressions in (15) are

$$I_1 = (I_{11} - \mu I_{12}), \quad I_4 = (I_{41} - \mu I_{42}),$$

$$I_{11} = \int_0^1 \Phi_1^2 \, \mathrm{d}s = 1,$$

$$I_{41} = \int_0^1 \Phi_1 \left(\Phi_{1s} \int_1^s \int_0^s \Phi_{1s}^2 \, \mathrm{d}s \, \mathrm{d}s \right)_s \mathrm{d}s,$$

$$\int_0^1 \Phi_1 \Phi_{1ssss} \, \mathrm{d}s = \omega_1^2 \int_0^1 \Phi_1^2 \, \mathrm{d}s = \omega_1^2 I_{11},$$

$$I_{42} = \int_0^1 \Phi_1 \left(\Phi_{1s}^3 \right)_s \mathrm{d}s,$$

$$I_{12} = \int_0^1 \Phi_1 \Phi_{1ss} \, \mathrm{d}s,$$

$$I_5 = \int_0^1 \Phi_1 \left(\Phi_{1s} (s-1) \right)_s \mathrm{d}s = \int_0^1 \Phi_{1s}^2 (1-s) \, \mathrm{d}s,$$

$$I_2 = \int_0^1 \Phi_1 \, \mathrm{d}s,$$

$$I_6 = \int_0^1 \Phi_1 \left(\Phi_{1s}^3 (s-1) \right)_s \mathrm{d}s = \int_0^1 \Phi_{1s}^4 (1-s) \, \mathrm{d}s,$$

$$I_3 = \int_0^1 \Phi_1 \left(\Phi_{1s} \left(\Phi_{1s} \Phi_{1ss} \right)_s \right)_s \mathrm{d}s$$

$$= 2 \int_0^1 (\Phi_{1s} \Phi_{1ss})^2 \, \mathrm{d}s,$$

$$I_7 = \int_0^1 \Phi_1 \left(\Phi_{1s} \int_1^s \left(\int_0^s \Phi_{1s}^2 \, \mathrm{d}s \right)_{ss} \mathrm{d}s \right)_s \mathrm{d}s. \quad (45)$$

Appendix 2

MSM: second-order solution

Substitution of p_1 (36) in the second equation of (33), and elimination of secular terms yield

$$D_1 B = 0 \quad (46)$$

so that

$$B = B(T_2, T_3), \quad p_2 = 0 \quad (47)$$

Using (36) and (47), and remembering that $\tilde{x}_{ref1} = A_{un}(T_1, T_2, T_3) e^{i\omega_1 T_0} + c.c.$ is the solution of amplitude $A_{un}(T_1, T_2, T_3)$ of the first-order uncontrolled system, the first equation of (33), without $\tilde{x}_{ref2}$ and $N_{22}(\tilde{x}_{ref1})$ terms, becomes

$$D_0^2 y_2 + \omega_1^2 y_2$$
$$= -2C_{214} \left(A\bar{A} + A\bar{A}_{un} \right) - C_{212} B^2$$
$$- e^{i\omega_1 T_0} \left(C_{213} (A + A_{un}) B + 2i\omega_1 D_1 A \right)$$
$$- C_{211} e^{2i\omega_1 T_0} \left(A^2 + 2AA_{un} \right) + c.c. \quad (48)$$

and the solvability condition implies that

$$D_1 A = \frac{iC_{213}}{2\omega_1} (A + A_{un}) B \quad (49)$$

For the uncontrolled system, it is $D_1 A_{un} = 0$ and thus $A_{un} = A_{un}(T_2, T_3)$. The particular solution at this order is

$$y_2 = \frac{C_{211}}{3\omega_1^2} \left(A^2 + 2AA_{un} \right) e^{2i\omega_1 T_0}$$
$$- \frac{2C_{214}}{\omega_1^2} \left(A\bar{A} + A\bar{A}_{un} \right) - \frac{C_{212}}{\omega_1^2} B^2 + c.c. \quad (50)$$

while the solution of the uncontrolled system is $\tilde{x}_{ref2} = \frac{C_{211}}{3\omega_1^2} A_{un}^2 e^{2i\omega_1 T_0} - \frac{2C_{214}}{\omega_1^2} A_{un}\bar{A}_{un} + c.c.$. For the expression of the C_{ijk} coefficients, see "Appendix 3" of [37].

MSM: third-order solution

At the third order, by means of the obtained results, the second of (34) becomes

$$D_0 p_3 = -D_2 B + \hat{k}_g C_{11} B/\omega_1^2 - \hat{k}_g A e^{i\omega_1 T_0} + c.c. \tag{51}$$

and the secular terms elimination, providing

$$D_2 B = \hat{k}_g C_{11} B/\omega_1^2, \tag{52}$$

permits to obtain

$$p_3 = \frac{i\hat{k}_g A e^{i\omega_1 T_0}}{\omega_1} + c.c. \tag{53}$$

Here, $\tilde{x}_{ref3}$ and $N_{32}(\tilde{x}_{ref1}, \tilde{x}_{ref2})$ terms, together with terms related to the horizontal and vertical excitations, are present also in the uncontrolled system, so that they can be neglected; using (36), (46), (47), (49), (50), (52), (53), and being $D_1 A_{un} = 0$ ("Appendix 2" of [37]), the first equation of (34) hence becomes

$$\begin{aligned} &D_0^2 y_3 + \omega_1^2 y_3 \\ &= \gamma_{31} e^{i\omega_1 T_0} + \gamma_{32} e^{2i\omega_1 T_0} + \gamma_{33} e^{3i\omega_1 T_0} + \gamma_{35} B^3 \\ &\quad + \gamma_{36}\left(A\bar{A} + \bar{A}A_{un} + A\bar{A}_{un} + A_{un}\bar{A}_{un}\right) B \\ &\quad + \gamma_{37}\left(\bar{A} + \bar{A}_{un}\right) D_1 A + c.c. \end{aligned} \tag{54}$$

with γ_{ij} defined in "Appendix 3" of [37]. Note that γ_{31} depends on $D_2 A$, so that the solvability condition of (54) provides

$$\begin{aligned} D_2 A = &-\frac{C_{35}\omega_1^2 + C_{11}\hat{k}_g}{2\omega_1^2} A \\ &+ i\frac{C_{301}\left(A^2\bar{A} + 2A\bar{A}A_{un} + \bar{A}A_{un}^2 + A^2\bar{A}_{un} + 2AA_{un}\bar{A}_{un}\right)}{2\omega_1} \\ &+ i\frac{C_{302}\left(AB^2 + A_{un}B^2\right)}{2\omega_1} \end{aligned} \tag{55}$$

The particular solution at the third order for the controlled system results

$$\begin{aligned} y_3 = &C_{306}B^3 + C_{303}\left(A^3 + 3A^2 A_{un} + 3AA_{un}^2\right) e^{3i\omega_1 T_0} \\ &+ C_{304}\left(A^2 B + 2AA_{un}B + A_{un}^2 B\right) e^{2i\omega_1 T_0} \\ &+ C_{305}\left(A\bar{A}B + A_{un}\bar{A}B + AB\bar{A}_{un} + A_{un}B\bar{A}_{un}\right) \\ &+ c.c. \end{aligned} \tag{56}$$

For what concerns the uncontrolled system, the solvability condition at the third order yields

$$\begin{aligned} D_2 A_{un} = &-\frac{C_{35}}{2} A_{un} + i\frac{C_{301}}{2\omega_1}\left(A_{un}^2\bar{A}_{un}\right) \\ &+ \frac{C_{sv}}{4\omega_1} e^{i\sigma_v T_2} + \frac{C_{su}}{4\omega_1} e^{i(\sigma_u T_2 + \phi_u)} \\ &+ i\frac{C_{cu}}{4\omega_1} e^{i(\sigma_u T_2 + \phi_u)} \end{aligned}$$

whose expression is later on needed, and the particular solution results $\tilde{x}_{ref3} = C_{303} A_{un}^3 e^{3i\omega_1 T_0} + c.c.$

MSM: fourth-order solution

By means of the previous results, the second equation of (35) at the fourth order becomes

$$\begin{aligned} &D_0 p_4 \\ &= -D_3 B - i\frac{\hat{k}_g}{\omega_1} D_1 A e^{i\omega_1 T_0} \\ &\quad + \frac{2C_{214}\hat{k}_g}{\omega_1^2}\left(A\bar{A} + A_{un}\bar{A} + A\bar{A}_{un}\right) + \frac{C_{212}\hat{k}_g}{\omega_1^2} B^2 \\ &\quad - \frac{C_{211}\hat{k}_g}{2\omega_1^2}\left(A^2 + 2AA_{un}\right) e^{2i\omega_1 T_0} + c.c. \end{aligned} \tag{57}$$

with the vanishing of secular term providing

$$\begin{aligned} D_3 B = &+\frac{2C_{214}\hat{k}_g}{\omega_1^2}\left(A\bar{A} + A_{un}\bar{A} + A\bar{A}_{un}\right) \\ &+ \frac{C_{212}\hat{k}_g}{\omega_1^2} B^2 \end{aligned} \tag{58}$$

and the particular solution resulting

$$\begin{aligned} p_4 = &-\frac{iC_{213}\hat{k}_g}{2\omega_1^3}\left(AB + A_{un}B\right) e^{i\omega_1 T_0} \\ &+ \frac{iC_{211}\hat{k}_g}{3\omega_1^3}\left(A^3 + 2AA_{un}\right) e^{2i\omega_1 T_0} + c.c. \end{aligned} \tag{59}$$

The first equation of (35) can thus be rewritten as

$$\begin{aligned} &D_0^2 y_4 + \omega_1^2 y_4 \\ &= -A^2\left(\gamma_{47}\bar{A}^2 + 2\gamma_{47}\bar{A}\bar{A}_{un} + \gamma_{47}\bar{A}_{un}^2\right) \\ &\quad - 4\gamma_{47}AA_{un}\bar{A}\bar{A}_{un} - A\left(B^2\left(\gamma_{45}\bar{A} + \gamma_{45}\bar{A}_{un}\right)\right. \\ &\quad \left. + \gamma_{49}\bar{A}_{un} + \gamma_{54}e^{-i\sigma_v T_2} + \gamma_{55}e^{-i\sigma_u T_2 - i\phi_u}\right) \\ &\quad - 2\gamma_{47}A_{un}^2\bar{A}\bar{A}_{un} - \gamma_{45}A_{un}B^2\bar{A}_{un} \\ &\quad - B\left(\gamma_{48}\bar{A}D_1 A + \gamma_{48}\bar{A}_{un}D_1 A\right) \\ &\quad - \gamma_{57}\bar{A}D_1^2 A - \gamma_{56}\bar{A}D_2 A \end{aligned}$$

$$
\begin{aligned}
&- \gamma_{56}\bar{A}D_2A_{un} - \gamma_{57}\bar{A}_{un}D_1^2A \\
&- \gamma_{56}\bar{A}_{un}D_2A - \gamma_{50}D_1AD_1\bar{A} \\
&- \gamma_{46}B^4 - \gamma_{41}e^{i\omega_1T_0} - \gamma_{42}e^{2i\omega_1T_0} \\
&- \gamma_{43}e^{3i\omega_1T_0} - \gamma_{44}e^{4i\omega_1T_0} + c.c. \qquad (60)
\end{aligned}
$$

The secular terms elimination requires that γ_{41}, which depends on D_3A, identically vanishes. Using Eqs. (46),(49),(52),(55), and assuming that $2D_1D_2A = \frac{\mathrm{d}D_1A}{\mathrm{d}T_2} + \frac{\mathrm{d}D_2A}{\mathrm{d}T_1}$ [39], it results

$$
\begin{aligned}
D_3A = {} & B^3(\gamma_{402}A + \gamma_{402}A_{un}) \\
& + B\Big(\gamma_{401}A^2\bar{A} + \gamma_{401}A^2\bar{A}_{un} \\
& + 2\gamma_{401}A\bar{A}A_{un} + 2\gamma_{401}AA_{un}\bar{A}_{un} \\
& + \gamma_{404}A + \gamma_{403}A_{un} \\
& + \gamma_{401}\bar{A}A_{un}^2 + \gamma_{401}A_{un}^2\bar{A}_{un} \\
& + \gamma_{405}e^{i\sigma_uT_2+i\phi_u} + \gamma_{406}e^{i\sigma_vT_2}\Big) \qquad (61)
\end{aligned}
$$

Appendix 3

Terms c_{hk}, $h,k = 1,\ldots,5$ of the Jacobian matrix (42) are

$$
\begin{aligned}
c_{11} = {} & \frac{1}{2}(b(2\beta_5 - \beta_1(j+j_{un})(n+n_{un})) \\
& - \beta_4(j(n+n_{un}) + j_{un}n)) \\
c_{12} = {} & \frac{1}{4}(-4\beta_2b^3 - 4\beta_3b^2 - b(\beta_1((j+j_{un})^2 \\
& + 3(n+n_{un})^2) + 4\beta_7) \\
& - \beta_4(j^2 + 2jj_{un} + 3n(n+2n_{un}))) \\
c_{13} = {} & \frac{1}{2}(b(2\beta_6 - \beta_1(j+j_{un})(n+n_{un})) \\
& - \beta_4(j+j_{un})(n+n_{un}) + 2\beta_9) \\
c_{14} = {} & \frac{1}{4}(-4\beta_2b^3 - 4\beta_3b^2 \\
& - b(\beta_1((j+j_{un})^2 + 3(n+n_{un})^2) + 4\beta_7) \\
& - \beta_4((j+j_{un})^2 + 3(n+n_{un})^2) + 4\omega_1(\Omega_u - 1)) \\
c_{15} = {} & \frac{1}{4}(-(n+n_{un})(12\beta_2b^2 \\
& + 8\beta_3b + \beta_1((j+j_{un})^2 + (n+n_{un})^2) \\
& + 4\beta_7) + 4\beta_5j_{un} + 4\beta_6j + 8\beta_8) \qquad (62)
\end{aligned}
$$

$$
\begin{aligned}
c_{21} = {} & \frac{1}{4}(4\beta_2b^3 + 4\beta_3b^2 \\
& + b(\beta_1(3(j+j_{un})^2 + (n+n_{un})^2) + 4\beta_7) \\
& + \beta_4(3j(j+2j_{un}) + n(n+2n_{un})))
\end{aligned}
$$

$$
\begin{aligned}
c_{22} = {} & \frac{1}{2}(b(\beta_1(j+j_{un})(n+n_{un}) + 2\beta_5) \\
& + \beta_4n(j+j_{un}) + \beta_4jn_{un}) \\
c_{23} = {} & \frac{1}{4}(4\beta_2b^3 + 4\beta_3b^2 \\
& + b(\beta_1(3(j+j_{un})^2 + (n+n_{un})^2) + 4\beta_7) \\
& + \beta_4(3(j+j_{un})^2 + (n+n_{un})^2) - 4\omega_1(\Omega_u - 1)) \\
c_{24} = {} & \frac{1}{2}(b(\beta_1(j+j_{un})(n+n_{un}) + 2\beta_6) \\
& + \beta_4(j+j_{un})(n+n_{un}) + 2\beta_9) \\
c_{25} = {} & \frac{1}{4}((j+j_{un})(12\beta_2b^2 + 8\beta_3b \\
& + \beta_1((j+j_{un})^2 + (n+n_{un})^2) \\
& + 4\beta_7) + 8\beta_{10} + 4(\beta_5n_{un} + \beta_6n)) \\
c_{31} = {} & \frac{C_{214}k_gj}{\omega_1^2} \\
c_{32} = {} & \frac{C_{214}k_gn}{\omega_1^2} \\
c_{33} = {} & \frac{1}{\omega_1^2}C_{214}k_g(j+j_{un}) \\
c_{34} = {} & \frac{1}{\omega_1^2}C_{214}k_g(n+n_{un}) \\
c_{35} = {} & \frac{1}{\omega_1^2}k_g(2C_{212}b + C_{11}) \\
c_{41} = {} & -\frac{1}{4}\left(\frac{C_{301}j_{un}n_{un}}{\omega_1} - 2C_{35}\right) \\
c_{42} = {} & \omega_1(\Omega_u - 1) - \frac{C_{301}(j_{un}^2 + 3n_{un}^2)}{8\omega_1} \\
c_{51} = {} & \frac{C_{301}(3j_{un}^2 + n_{un}^2)}{8\omega_1} - \omega_1(\Omega_u - 1) \\
c_{52} = {} & \frac{1}{4}\left(\frac{C_{301}j_{un}n_{un}}{\omega_1} - 2C_{35}\right)
\end{aligned}
$$

Appendix 4

Coefficients f_{hkl} of the steady-state responses (41) are

$$
\begin{aligned}
f_{y0} = {} & -\frac{C_{214}(j^2 + 2jj_{un} + n^2 + 2nn_{un})}{2\omega_1^2} \\
& + C_{306}b^3 - \frac{C_{212}}{\omega_1^2}b^2 \\
& + \left(\frac{1}{4}C_{305}((j+j_{un})^2 + (n+n_{un})^2) - \frac{C_{11}}{\omega_1^2}\right)b \\
f_{yc1} = {} & j \\
f_{ys1} = {} & -n
\end{aligned}
$$

$$f_{yc2} = +\Big(\frac{C_{211}(j^2+2jj_{un}-n(n+2n_{un}))}{6\omega_1^2} + \frac{1}{2}C_{304}(j+j_{un}-n-n_{un})(j+j_{un}+n+n_{un})b\Big)$$

$$f_{ys2} = -\Big(C_{304}(j+j_{un})(n+n_{un})b + \frac{C_{211}(j(n+n_{un})+j_{un}n)}{3\omega_1^2}\Big)$$

$$f_{yc3} = +\frac{1}{4}C_{303}\Big(j^3+3j^2j_{un}+3j(j_{un}^2-(n+n_{un})^2) - 3j_{un}n(n+2n_{un})\Big)$$

$$f_{ys3} = +\frac{1}{4}C_{303}\Big(-3j^2(n+n_{un})-6jj_{un}(n+n_{un}) + n(-3j_{un}^2+n^2+3nn_{un}+3n_{un}^2)\Big)$$

$$f_{z0} = b$$

$$f_{zc1} = -\frac{k_g n}{\omega_1}$$

$$f_{zs1} = -\frac{k_g j}{\omega_1}$$

References

1. Lee, S.I., Howell, S.A.R.: Nonlinear dynamic perspectives on dynamic force microscopy. Ultramicroscopy **97**, 185–198 (2003)
2. Couturier, G., Boisgard, R.J.-P.: Noncontact atomic force microscopy: stability criterion and dynamical responses of the shift of frequency and damping signal. Rev. Sci. Instrum. **74**(5), 2726–2734 (2003)
3. Yagasaki, K.: Nonlinear dynamics of vibrating microcantilevers in tapping-mode atomic force microscopy. Phys. Rev. B **70**, 245419 (2004)
4. Misra, S., Dankowicz, H.M.R.: Degenerate discontinuity-induced bifurcations in tapping-mode atomic-force microscopy. Phys. D **239**, 33–43 (2010)
5. Bahrami, A., Nayfeh, A.H.: On the dynamics of tapping mode atomic force microscope probes. Nonlinear Dyn. **70**, 1605–1617 (2012)
6. Hornstein, S., Gottlieb, O.: Nonlinear dynamics, stability and control of the scan process in noncontacting atomic force microscopy. Nonlinear Dyn. **54**, 93–122 (2008)
7. Rega, G., Settimi, V.: Bifurcation, response scenarios and dynamic integrity in a single-mode model of noncontact atomic force microscopy. Nonlinear Dyn. **73**, 101–123 (2013)
8. Burnham, N.A., Chen, X., Hodges, C.S., Matei, G.A., Thoreson, E.J., Roberts, C.J., Davies, M.C., Tendler, S.J.B.: Comparison of calibration methods for atomic-force microscopy cantilevers. Nanotechnology **14**, 1–6 (2003)
9. Lübbe, J., Temmen, M., Rode, S., Rahe, P., Kühnle, A., Reichling, M.: Thermal noise limit for ultra-high vacuum noncontact atomic force microscopy. Beilstein J. Nanotechnol. **4**, 32–44 (2013)
10. Slattery, A.D., Blanch, A.J., Quinton, J.S., Gibson, C.T.: Accurate measurement of atomic force microscope cantilever deflection excluding tip-surface contact with application to force calibration. Ultramicroscopy **131**, 46–55 (2013)
11. Heima, L.-O., Rodrigues, T.S., Bonaccurso, E.: Direct thermal noise calibration of colloidal probe cantilevers. Colloids Surf. A Physicochem. Eng. Asp. **443**, 377–383 (2014)
12. Humphris, A.D.L., Tamayo, J., Miles, M.J.: Active quality factor control in liquids for force spectroscopy. Langmuir **16**, 7891–7894 (2000)
13. Zou, Q., Leang, K.K., Sadoun, E., Reed, M.J., Devasia, S.: Control issues in high-speed afm for biological applications: collagen imaging sample. Asian J. Control. **6**(2), 164–178 (2004)
14. Yamasue, K., Hikihara, T.: Control of microcantilevers in dynamic force microscopy using time delayed feedback. Rev. Sci. Instrum. **77**, 053703 (2006)
15. Arjmand, M.T., Sadeghian, H., Salarieh, H., Alasty, A.: Chaos control in afm systems using nonlinear delayed feedback via sliding mode control. Nonlinear Anal. Hybrid Syst. **2**, 993–1001 (2008)
16. Merry, R., Uyanik, M., van de Molengraft, R., Koops, R., van Veghel, M., Steinbuch, M.: Identification, control and hysteresis compensation of a 3 dof metrological afm. Asian J. Control. **11**(2), 130–143 (2009)
17. Payton, O., Champneys, A.R., Homer, M.E., Picco, L., Miles, M.J.: Feedback-induced instability in tapping mode atomic force microscopy: theory and experiment. Proc. R. Soc. A **467**(2130), 1801–1822 (2011). doi:10.1098/rspa.2010.0451
18. Salarieh, H., Alasty, A.: Control of chaos in atomic force microscopes using delayed feedback based on entropy minimization. Commun. Nonlinear Sci. Numer. Simul. **14**, 637–644 (2009)
19. Wang, C.C., Pai, N.S., Yau, H.T.: Chaos control in afm system using sliding mode control by backstepping design. Commun. Nonlinear Sci. Numer. Simul. **15**, 741–751 (2010)
20. Yamasue, K., Kobayashi, K., Yamada, H., Matsushige, K., Hikihara, T.: Controlling chaos in dynamic-mode atomic force microscope. Phys. Lett. A **373**(35), 3140–3144 (2009). doi:10.1016/j.physleta.2009.07.009
21. Yagasaki, K.: New control methodology of microcantilevers in atomic force microscopy. Phys. Lett. A **375**, 23–28 (2010)
22. Pyragas, K.: Continuous control of chaos by self-controlling feedback. Phys. Lett. A **170**, 421–428 (1992)
23. Yagasaki, K.: Nonlinear dynamics and bifurcations in external feedback control of microcantilevers in atomic force microscopy. Commun. Nonlinear Sci. Numer. Simul. **18**(10), 2926–2943 (2013)
24. Crespo da Silva, M.R.M., Glynn, C.C.: Nonlinear flexural-flexural-torsional dynamics of inextensional beams. i. Equations of motion. Mech. Based Des. Struct. Mach. **6**(4), 437–448 (1978)
25. Israelachvili, J.: Intermolecolar and Surface Forces. Academic Press, London (1992)
26. Sarid, D., Ruskell, T.G., Workman, R.K., Chen, D.: Driven nonlinear atomic force microscopy cantilevers: from noncontact to tapping modes of operation. J. Vac. Sci. Technol. B **14**(2), 864–867 (1996)
27. Butt, H.J., Graf, K., Kappl, M.: Physics and Chemistry of Interfaces.Wiley-VCH, Weinheim (2003)

28. Hu, S., Howell, S., Raman, A., Reifenberger, R., Franchek, M.: Frequency domain identification of tip-sample van der Waals interactions in resonant atomic force microcantilevers. J. Vib. Acoust. **126**, 343–351 (2004)
29. Rodriguez, R.D., Lacaze, E., Jupille, J.: Probing the probe: AFM tip-profiling via nanotemplates to determine Hamaker constants from phase-distance curves. Ultramicroscopy **121**, 25–30 (2012)
30. Kuhn, S., Rahe, P.: Discriminating short-range from van der Waals forces using total force data in noncontact atomic force microscopy. Phys. Rev. B **89**, 235417 (2014)
31. Nayfeh, A.H., Mook, D.T.: Nonlinear Oscillations. Wiley, New York (1979)
32. Rodriguez, T.R., García, R.: Compositional mapping of surfaces in atomic force microscopy by excitation of the second normal mode of the microcantilever. Appl. Phys. Lett. **84**(3), 449 (2004)
33. Sahin, O., Quate, C.F., Solgaard, O., Atalar, A.: Resonant harmonic response in tapping-mode atomic force microscopy. Phys. Rev. B **69**, 165416 (2004)
34. Hornstein, S., Gottlieb, O.: Nonlinear multimode dynamics and internal resonances of the scan process in noncontacting atomic force microscopy. J. Appl. Phys. **112**, 074314 (2012)
35. Maali, A., Hurth, C., Boisgard, R., Jai, C., Cohen-Bouhacina, T., Aimé, J.P.: Hydrodynamics of oscillating atomic force microscopy cantilevers in viscous fluids. J. Appl. Phys. **97**, 074907 (2005)
36. Hölscher, H., Milde, P., Zerweck, U., Eng, L.M., Hoffmann, R.: The effective quality factor at low temperatures in dynamic force microscopes with Fabry-Pérot interferometer detection. Appl. Phys. Lett. **94**, 223514 (2009)
37. Settimi, V.: Bifurcation scenarios, dynamical integrity and control of noncontact atomic force microscopes. PhD thesis, Sapienza, University of Rome, 2013. http://hdl.handle.net/10805/2146
38. Nayfeh, A.H.: Perturbation methods in nonlinear dynamics. In: Jowett, J.M., Month, M., Turner, S. (eds.) Nonlinear Dynamics Aspects of Particle Accelerators, Springer-Verlag, New York (1985)
39. Luongo, A., Zulli, D.: A paradigmatic system to study the transition from zero/Hopf to double-zero/Hopf bifurcation. Nonlinear Dyn. **70**, 111–124 (2012)